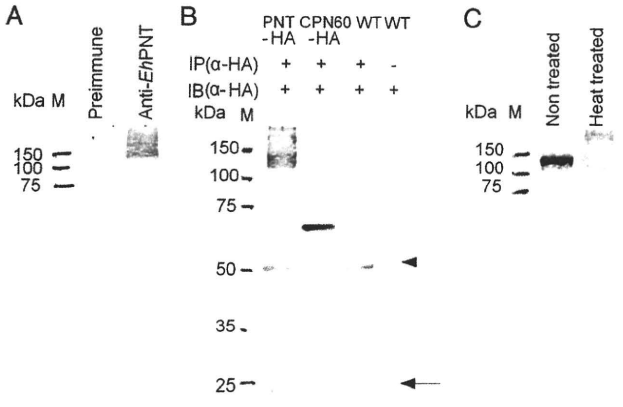

FIG. 1. Expression of PNT in *E. histolytica*. (A) Immunoblot analysis of native *Eh*PNT. Approximately 10 μg of total lysate was electrophoresed on a 12% SDS-polyacrylamide gel and subjected to an immunoblot assay with anti-*Eh*PNT antibody or preimmune serum. M, molecular mass marker. (B) Immunoprecipitation of *Eh*PNT. The lysates derived from the transformant expressing either *Eh*PNT-HA ("PNT-HA") or *Eh*Cpn60-HA ("CPN60-HA") and the wild-type strain ("WT") were subjected to immunoprecipitation with anti-HA antibody, followed by immunoblot analysis with anti-HA antibody. Lysate derived from the wild-type amoebae was also used directly for immunoblot analysis as a control. An arrowhead and an arrow indicate heavy and light chains of anti-HA antibody, respectively. IP, immunoprecipitation; IB, immunoblot. (C) Effect of heat treatment on the mobility of *Eh*PNT on an SDS-PAGE gel. Approximately 10 μg of total lysate was electrophoresed on a 12% SDS-polyacrylamide gel and subjected to an immunoblot assay with anti-*Eh*PNT antibody. M, molecular mass marker.

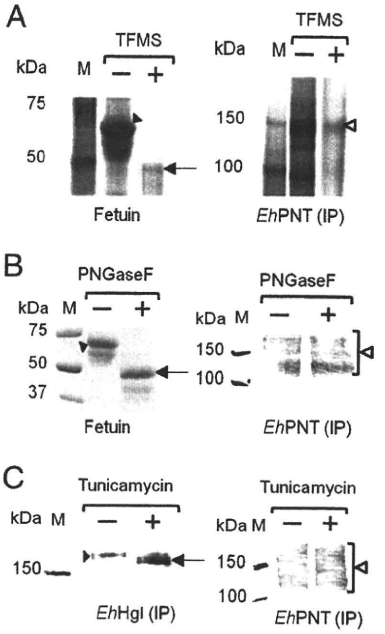

FIG. 2. Deglycosylation of *Eh*PNT. (A and B) Deglycosylation by TFMS or PNGase F. The lysates obtained from the transformant expressing *Eh*PNT-HA were subjected to immunoprecipitation (IP) with anti-HA antibody, followed by TFMS or PNGase F treatment and immunoblot detection with anti-HA antibody (right). Fetuin was used as a control, and gels were stained with silver (A) or Coomassie brilliant blue (B) (left). Filled arrowheads indicate untreated fetuin. Arrows indicate fetuin deglycosylated by TFMS (A) or PNGase F (B). Open arrowheads indicate *Eh*PNT. (C) Deglycosylation by tunicamycin. Lysates from the transformant expressing *Eh*PNT-HA cultured with tunicamycin were subjected to immunoprecipitation with either anti-*Eh*Hgl or anti-HA antibody, followed by immunoblot analysis with either anti-*Eh*Hgl or anti-HA antibody, respectively. A filled arrowhead or an arrow indicates untreated or deglycosylated *Eh*Hgl, respectively. An open arrowhead indicates *Eh*PNT.

(8). The dIII, dI, and dIIa regions of EHI_055400 (1,098 aa) are conserved except for a single amino acid substitution in dIII. EHI_055400 also contains a 5-aa extension at the amino terminus (MSLLL) and 9 aa substitutions in the putative TS (aa 1 to 14 of EHI_014030) (data not shown). In addition, dIIb of EHI_055400 contained 65 aa substitutions and two (4- and 6-aa-long) block insertions; the linker region also contains 24 aa substitutions. Since the domains involved in catalysis in EHI_055400 and EHI_014030 are totally conserved, and the two genes are expressed at comparable levels as steady-state mRNA by quantitative reverse transcriptase PCR (data not shown), we further studied only EHI_014030 in the present work. EHI_001930 (GenBank accession number XP_653216), which is annotated as the PNT β-subunit, showed no significant homology to either of the two *Eh*PNTs described above, while this sequence showed similarity with the β-subunit from other organisms and, thus, was excluded from this study.

Expression of PNT in *E. histolytica* trophozoites. Immunoblot analysis of the trophozoite lysate using anti-*Eh*PNT antibody showed a smear of >120 kDa (Fig. 1A). The size of the smear was unexpected because the predicted molecular masses of EHI_055400 and EHI_014030 were 119.0 and 117.0 kDa, respectively. To verify that this was not due to the cross-reactivity of anti-*Eh*PNT antibody, we immunoprecipitated *Eh*PNT from the *Eh*PNT-HA-expressing transformant with anti-HA antibody, followed by immunoblotting with anti-HA (Fig. 1B) or anti-*Eh*PNT (data not shown) antibody. Immunoprecipitated *Eh*PNT-HA was also recognized as a smear of >120 kDa, similar to that of endogenous *Eh*PNT.

To examine whether the smear was due to posttranslational modifications such as glycosylation, we treated immunoprecipitated *Eh*PNT-HA with TFMS or PNGase F. The pattern of immunoblots with anti-HA antibody was not affected, while the apparent molecular mass of control fetuin decreased (Fig. 2A and B). In addition, the treatment of the trophozoites with tunicamycin did not affect the mobility of *Eh*PNT, while the mobility of control Hgl increased (Fig. 2C). These data are consistent with the notion that *Eh*PNT is not glycosylated. We next examined whether aberrant mobility is due to unusual tertiary structures. We compared the patterns of the amoebic lysates, mixed with a one-third volume of 4× SDS-PAGE sample buffer (0.25 M Tris-HCl [pH 6.8], 8% SDS, and 8% 2-mercaptoethanol) and either incubated at 95°C for 5 min or left unheated, on SDS-PAGE gels. When the sample was electrophoresed without heating, *Eh*PNT was observed as a polypeptide of the predicted size (Fig. 1C). The exclusion of 2-mercaptoethanol did not affect mobility (data not shown). A similar observation was previously reported for membrane proteins, including serotonin transporter (24) and severe acute respiratory syndrome (SARS)-associated coronavirus mem-

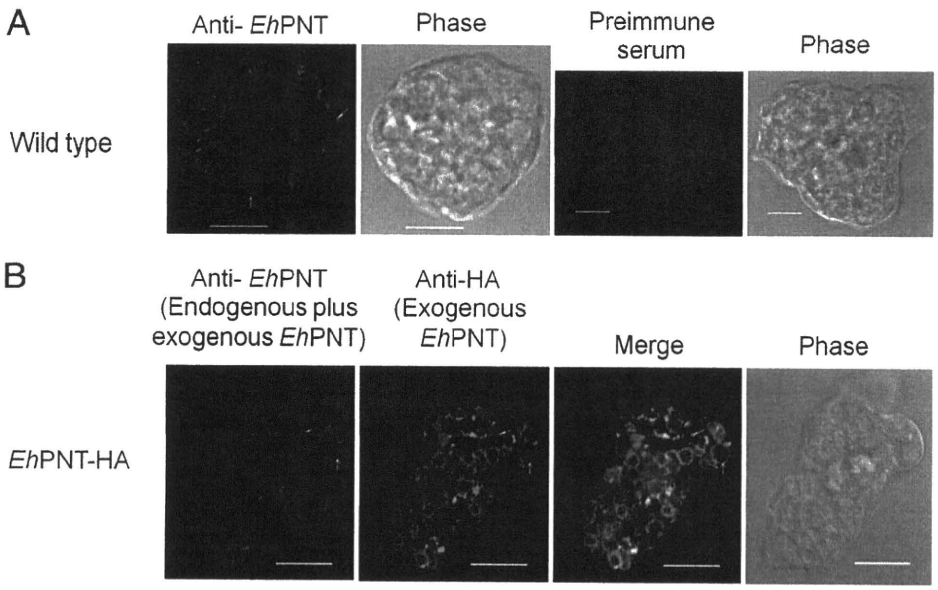

FIG. 3. (A) Subcellular localization of *Eh*PNT in wild-type amoebae. Wild-type amoebae were fixed, and an immunofluorescence assay was performed by using anti-*Eh*PNT (red) and preimmune sera. Bar, 10 μm. Arrows and arrowheads indicate representative vacuolar and dot-like structures of *Eh*PNT, respectively. (B) Colocalization of endogenous and exogenous epitope-tagged PNT in *E. histolytica*. *Eh*PNT-HA-overexpressing amoebae were fixed, and an immunofluorescence assay was performed by using anti-*Eh*PNT (red) and anti-HA (green) antibodies.

brane protein (18). In the latter case, three hydrophobic regions of 10 to 35 aa were shown to be responsible for the heat-induced aggregation of the membrane protein (18), suggesting that the heat-induced change of mobility of *Eh*PNT on SDS-PAGE is likely due to the hydrophobic nature of the protein.

Subcellular distribution of *Eh*PNT. An immunofluorescence assay using anti-*Eh*PNT antibody showed that *Eh*PNT is associated with the membranes of vesicles and vacuoles varying in size, or sometimes dot-like structures, scattered throughout the cytosol (Fig. 3A). We also examined the intracellular distribution of *Eh*PNT using the amoebic transformant that expressed *Eh*PNT (EHI_014030) with the carboxyl-terminal HA tag. The pattern of exogenous *Eh*PNT-HA (EHI_014030) and that of endogenous *Eh*PNT (a sum of EHI_055400 and EHI_014030) plus exogenous *Eh*PNT (EHI_014030) were indistinguishable (Fig. 3B). Since *Eh*PNT was previously postulated to be localized to mitosomes (8), we next examined the localization of *Eh*PNT and *Eh*Cpn60, the authentic marker of mitosomes, in the amoebic transformant expressing *Eh*Cpn60-HA (26) using anti-*Eh*PNT and anti-HA antibodies. No colocalization of *Eh*PNT and *Eh*Cpn60 was observed (Fig. 4).

Since *Eh*PNT was previously detected in isolated phagosomes (32, 33), we examined the localization of *Eh*PNT during the phagocytosis of CHO cells. Wild-type amoebae were incubated with CellTracker Orange-loaded CHO cells for 10 to 60 min to allow the ingestion of CHO cells. An immunofluorescence assay using anti-*Eh*PNT antibody (Fig. 5A) showed that the phagocytosed CHO cells were associated with *Eh*PNT at all time points (10, 20, and 60 min; only the images at 60 min are shown). The percentage of association gradually increased during the course of phagocytosis (65% ± 6%, 79% ± 9%, and 80% ± 8% at 10, 30, and 60 min, respectively). We then examined whether *Eh*PNT is localized to lysosomes using LysoTracker Red, a membrane-diffusible probe accumulated in acidic organelles (5). We found that the LysoTracker-labeled acidic compartment, the size and number of which were consistent with previous findings (28, 36), was associated with *Eh*PNT under steady-state conditions (79% ± 6% association) (Fig. 5B). To see whether *Eh*PNT is also associated with endosomes, we examined the localization of an endocytosed

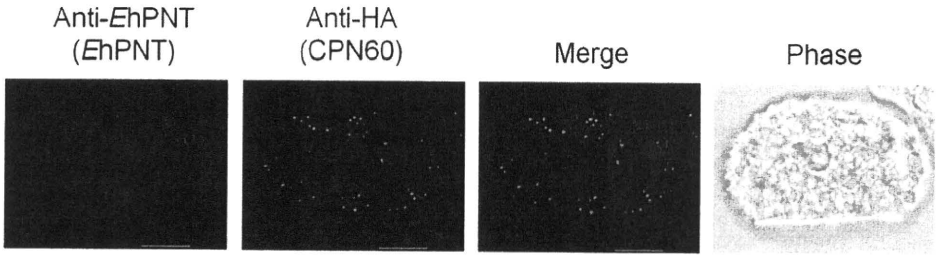

FIG. 4. Lack of association of *Eh*PNT with mitosomes. The amoebic transformant expressing *Eh*Cpn60-HA was stained with anti-HA (green) and anti-*Eh*PNT (red) antibodies to visualize *Eh*Cpn60 and *Eh*PNT, respectively. Bar, 10 μm.

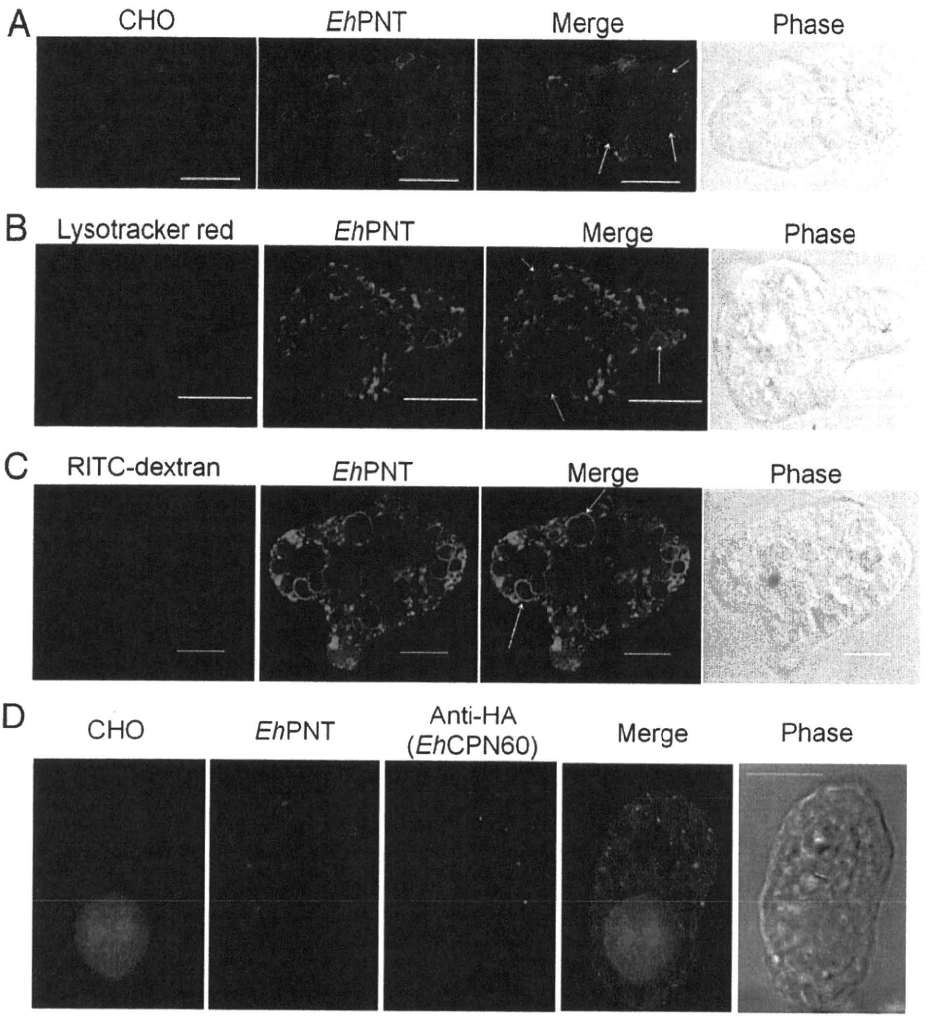

FIG. 5. Localization of *Eh*PNT to phagosomes, lysosomes, and endosomes. (A) Association of *Eh*PNT with phagosomes. Amoebae were incubated with CellTracker Orange-loaded CHO cells (red) for 60 min, fixed, and reacted with anti-*Eh*PNT antibody (green). Arrows indicate representative phagocytosed CHO cells associated with *Eh*PNT. (B) Association of *Eh*PNT with lysosomes. Amoebae were labeled with LysoTracker (red) and subjected to an immunofluorescence assay with anti-*Eh*PNT antibody (green). Arrows indicate representative lysosomes associated with *Eh*PNT. (C) Association of *Eh*PNT with the fluid-phase marker. Amoebae were incubated with medium containing RITC-dextran (red) for 1 h. The cells were fixed and reacted with anti-*Eh*PNT antibody (green). Arrows indicate representative endocytosed RITC-dextran associated with *Eh*PNT. (D) Subcellular localization of phagosomes, mitosomes, and *Eh*PNT. The amoebic transformant expressing *Eh*Cpn60-HA was incubated with CellTracker Blue-loaded CHO cells (blue) for 60 min, fixed, and reacted with anti-*Eh*PNT (red) and anti-*Eh*Cpn60 (green) antibodies. Bar, 10 μm.

fluid-phage marker, RITC-dextran. *Eh*PNT was only partially associated with RITC-dextran-containing endosomes, which were observed as tiny dot-like structures or a multivesicular body as previously shown (29), at each time point (10, 30, or 60 min; only the images at 60 min are shown) (Fig. 5C). We also examined whether *Eh*PNT is associated with mitosomes during the phagocytosis of CHO cells. An immunofluorescence assay using the amoebic transformant expressing *Eh*Cpn60-HA, CellTracker Blue-loaded CHO cells, anti-*Eh*PNT, and anti-HA antibody showed no colocalization of mitosomes and *Eh*PNT (Fig. 5D).

All domains are essential for the vesicular/vacuolar distribution of *Eh*PNT. To define the domain necessary for vesicular/vacuolar targeting of *Eh*PNT, we created amoeba transformants expressing the HA-tagged or GFP-fused protein containing various domains of PNT (Fig. 6A). The amoebic transformant expressing GFP fused with the 14-aa amino-terminal putative TS showed a cytoplasmic distribution (Fig. 6B), although the sequence MSTSSSIEEEVFNY appeared to contain the elements implicated for the TS (rich in hydroxylated and hydrophobic amino acids). The transformants expressing TS+dIIb-HA, TS+dIIb+dIII-HA, TS+dIIb+dIII+L-HA, or TS+dIIb+dIII+L+dI-HA showed a distribution that overlapped that of the endoplasmic reticulum (ER), visualized with anti-*Eh*Sec61 α-subunit antibody (27). The ER pattern was also confirmed with anti-*Eh*DPMS antibody (Fig. 6B). Full-length *Eh*PNT-HA did not overlap the ER visualized with either anti-*Eh*Sec61 α-subunit or anti-*Eh*DPMS antibody. Fractionation of the amoeba lysate followed by immunoblot analysis with anti-HA or anti-GFP an-

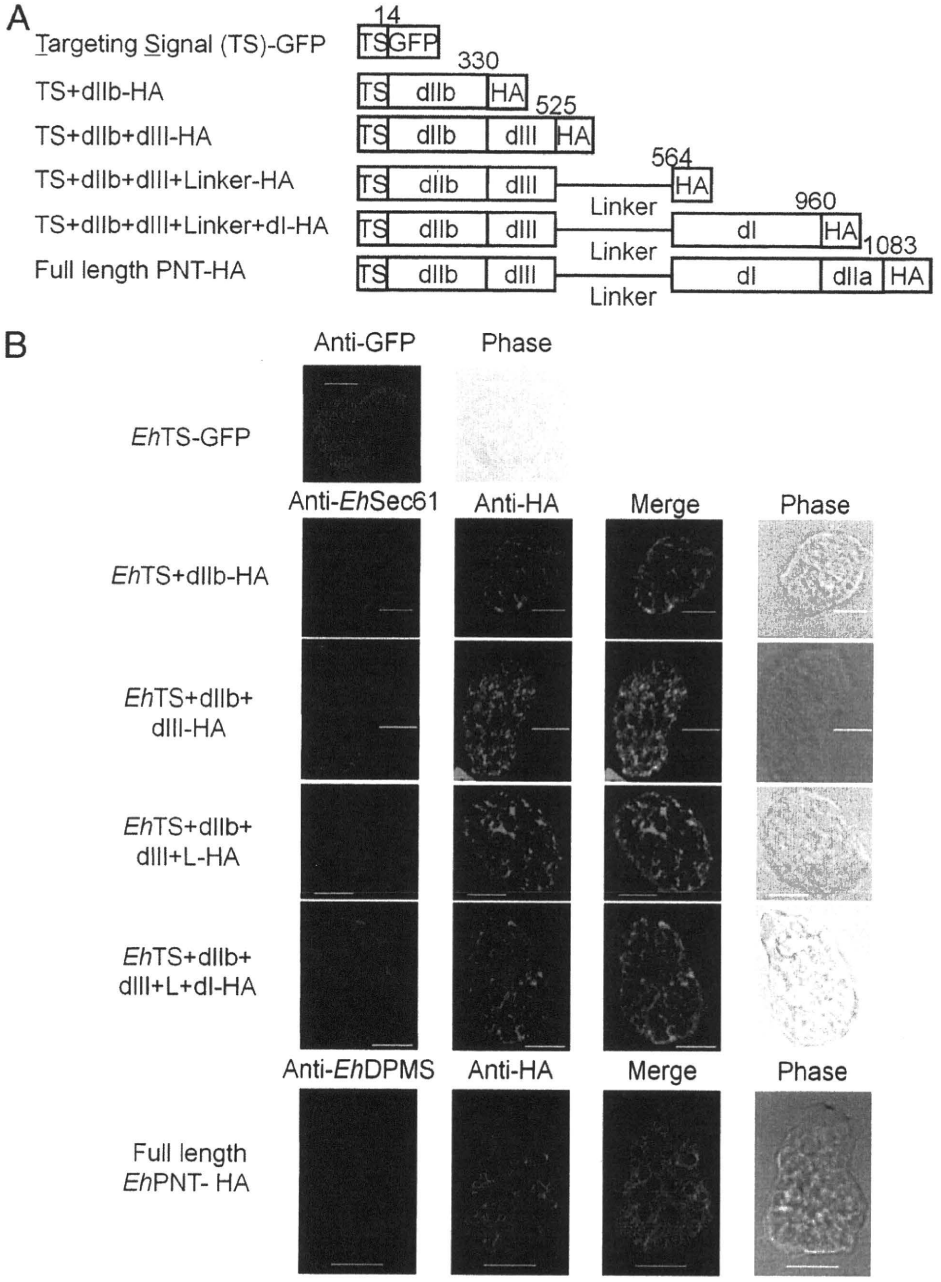

FIG. 6. Localization of a series of truncated *Eh*PNT proteins. (A) Schematic representation of HA epitope-tagged or GFP-fused recombinant *Eh*PNT used in the study. Domains, epitope (or GFP), and amino acid numbers are shown. (B) Localization of epitope-tagged or GFP-fused carboxyl-terminally truncated *Eh*PNT recombinant proteins. The transformants expressing *Eh*TS-GFP, *Eh*TS+dIIb-HA, *Eh*TS+dIIb+dIII-HA, *Eh*TS+dIIb+dIII+L-HA, and *Eh*TS+dIIb+dIII+L+dI-HA and *Eh*PNT-HA were subjected to an immunofluorescence assay using anti-HA (or anti-GFP for *Eh*TS-GFP) and anti-*Eh*Sec61 α-subunit (or anti-*Eh*DPMS for the *Eh*PNT-HA transformant) antibodies. Bar, 10 μm.

tibodies showed that all truncated forms of *Eh*PNT except for TS-GFP were partitioned into the 5,000 × *g* and 100,000 × *g* pellet fractions, while TS-GFP was fractionated into the 100,000 × *g* supernatant fraction (data not shown).

DISCUSSION

Mitosomes have been identified in several parasitic protozoan lineages such as *E. histolytica*, *Giardia intestinalis*, *Trachipleistophora hominis*, and *Cryptosporidium parvum* (21, 34, 42, 43, 50). *E. histolytica* was previously considered to be an early-branching "amitochondriate," as it lacks conventional mitochondria as well as other organelles typically found in most eukaryotes, such as peroxisomes, the rough ER, and the Golgi apparatus. However, the discovery of genes encoding the mitochondrial proteins Cpn60, PNT, mt-hsp70, ADP/ATP transporter, and Cpn10 (2, 7, 8, 21, 46) indicated that *E. histolytica* is the secondary "amito-

chondriate." While only a half-dozen proteins were shown to be localized to mitosomes (1, 2, 7, 8, 19, 21, 42, 44, 46), we recently discovered by proteomic analysis of isolated mitosomes that sulfate activation is the major pathway compartmentalized in mitosomes. Three enzymes consisting of the pathway and additional proteins required for the pathway, including sodium/sulfate symporter, mitochondrion carrier family protein, and chaperons, were identified in the mitosomal proteome. Although PNT was not discovered in the proteome, it was previously postulated to be mitosomal based on the resemblance of the amino-terminal region of *Eh*PNT to the potential mitochondrion-targeting peptide. However, it is important that the putative TS of *Eh*PNT is certainly not a canonical mitochondrion-targeting peptide because it lacks basic residues such as arginine or lysine.

Despite the premise, we showed, in this study, that *Eh*PNT was distributed to the membrane of vesicles and vacuoles, including lysosomes, phagosomes, and endosomes, but not to mitosomes. In addition, we showed that GFP fused with the amino-terminal putative TS of *Eh*PNT was distributed to the cytosol, which disproved the premise that the amino-terminal domain of *Eh*PNT functions as a putative organelle-targeting sequence. The 15-aa-long amino terminus of Cpn60 was not sufficient for the targeting of either luciferase or GFP to mitosomes (1; our unpublished data), although the removal of the first 15 aa of Cpn60 caused a mislocalization of the protein in the cytoplasm (42). Therefore, a role of the amino-terminal transit peptide for mitosomal transport remains obscure.

The association of PNT with the acidified compartments (lysosomes and phagosomes) (Fig. 5) is unprecedented in eukaryotes, where PNT is usually localized to the inner membrane of mitochondria (48). The dependence of transhydrogenase activity of *Eh*PNT on pH was demonstrated; the rate of transhydrogenation was higher at an acidic pH (5.5) than at a neutral pH (7.0 to 8.0) (49). The generation of NADPH by membrane-associated PNT (49) depends upon a proton-motive force, which is likely generated by V-ATPase localized to the acidified compartment and also the nonacidified compartment. While the colocalization of V-ATPase and *Eh*PNT has not been directly demonstrated, phagosomes contained major components of V-ATPase, as shown by the proteomic analysis of purified phagosomes (32, 33). Therefore, it is conceivable that amebic PNT localized in the acidic environment possesses enzymological properties suitable for acidic environments. Since our attempt to repress *Eh*PNT expression by gene silencing failed (our unpublished data), the physiological role of *Eh*PNT has not been elucidated. However, *Eh*PNT may be involved in the detoxification of reactive oxygen and nitrogen species by supplying NADPH as a reducing power by using a proton gradient across the lysosomal and phagosomal membranes. During tissue invasion, *E. histolytica* adapts to changing oxygen tensions as it goes from the anaerobic colonic lumen to an oxygen-rich environment in the tissue (40). Additionally, the parasite must cope with cytotoxic reactive oxygen and nitrogen species that are produced and released by activated phagocytes that are attracted to the site of infection (4, 20, 40).

Although we cannot exclude the possibility that truncated *Eh*PNT was misfolded and aggregated in the cell, our immunofluorescence and cellular fractionation data are consistent with the premise that all truncated *Eh*PNT was retained in the ER, which is suggestive of the default mechanisms of retention of multiple transmembrane proteins in the ER. The possibility that truncated *Eh*PNT is retained in the heavy microsomal fraction was previously suggested (1), where the majority (93%) of luciferase activity of the recombinant protein consisted of the 67-aa-long amino-terminal portion of PNT fused to firefly luciferase was associated with the mixed membrane fraction and was as susceptible to trypsin degradation as cytosolic luciferase from control parasites. Our present data also support the interpretation of the study that the fusion protein is embedded in the ER membrane and not targeted to mitosomes. We also showed that the aberrant mobility of PNT on SDS-PAGE gels (Fig. 1) was not likely due to either N-linked or O-linked glycosylation but was due to the hydrophobic nature of *Eh*PNT. Altogether, *E. histolytica* PNT represents a novel class of PNT localized to lysosomes and appears to have evolved uniquely in this organism.

ACKNOWLEDGMENTS

We thank Rosana Sánchez-López, Universidad Nacional Autónoma de México, for anti-*Eh*Sec61 α-subunit and anti-*Eh*DPMS antibodies and Barbara J. Mann and William A. Petri, Jr., University of Virginia Health System, for anti-Hgl antibody (3F4). We also thank Takashi Makiuchi for helpful discussions.

This work was supported by a grant-in-aid for creative scientific research (grant 18GS0314) and a grant-in-aid for scientific research (grants 18GS0314, 18050006, and 18073001) from the Ministry of Education, Culture, Sports, Science, and Technology of Japan to T.N.; a grant for Research on Emerging and Re-Emerging Infectious Diseases from the Ministry of Health, Labor, and Welfare of Japan (grant H20-Shinkosaiko-Ippan-016); and a grant for research to promote the development of anti-AIDS pharmaceuticals from the Japan Health Sciences Foundation to T.N. (grant KAA1551).

REFERENCES

1. **Aguilera, P., T. Barry, and J. Tovar.** 2008. *Entamoeba histolytica* mitosomes: organelles in search of a function. Exp. Parasitol. **118:**10–16.
2. **Bakatselou, C., C. Kidgell, and C. C. Clark.** 2000. A mitochondrial-type hsp70 gene of *Entamoeba histolytica*. Mol. Biochem. Parasitol. **110:**177–182.
3. **Bizouarn, T., O. Fjellstrom, J. Meuller, M. Axelsson, A. Bergkvist, C. Johansson, G. Karlsson, and J. Rydstrom.** 2000. Proton translocating nicotinamide nucleotide transhydrogenase from *E. coli*. Mechanism of action deduced from its structural and catalytic properties. Biochim. Biophys. Acta **1457:**211–228.
4. **Bogdan, C., M. Rollinghoff, and A. Diefenbach.** 2000. Reactive oxygen and reactive nitrogen intermediates in innate and specific immunity. Curr. Opin. Immunol. **12:**64–76.
5. **Bucci, C., P. Thomsen, P. Nicoziani, J. McCarthy, and B. van Deurs.** 2000. Rab7: a key to lysosome biogenesis. Mol. Biol. Cell **11:**467–480.
6. **Carlton, J. M., S. V. Angiuoli, and D. J. Carucci.** 2002. Genome sequence and comparative analysis of the model rodent malaria parasite *Plasmodium yoelii*. Nature **419:**512–519.
7. **Chan, K. W., D. J. Slotboom, S. Cox, T. M. Embley, O. Fabre, M. van der Giezen, M. Harding, D. S. Horner, E. R. Kunji, G. Leon-Avila, and J. Tovar.** 2005. A novel ADP/ATP transporter in the mitosome of the microaerophilic human parasite *Entamoeba histolytica*. Curr. Biol. **15:**737–742.
8. **Clark, C. G., and A. J. Roger.** 1995. Direct evidence for secondary loss of mitochondria in *Entamoeba histolytica*. Proc. Natl. Acad. Sci. U. S. A. **92:** 6518–6521.
9. **Diamond, L. S., D. R. Harlow, and C. C. Cunnick.** 1978. A new medium for the axenic cultivation of *Entamoeba histolytica* and other *Entamoeba*. Trans. R. Soc. Trop. Med. Hyg. **72:**431–432.
10. **Gardner, M. J., and B. Barrell.** 2002. Genome sequence of the human malaria parasite *Plasmodium falciparum*. Nature **419:**498–511.
11. **Gill, E. E., S. Diaz-Triviño, M. J. Barberà, J. D. Silberman, A. Stechmann, D. Gaston, I. Tamas, and A. J. Roger.** 2007. Novel mitochondrion-related organelles in the anaerobic amoeba *Mastigamoeba balamuthi*. Mol. Microbiol. **66:**1306–1320.
12. **Hall, N., M. Karras, and R. E. Sinden.** 2005. A comprehensive survey of the *Plasmodium* life cycle by genomic, transcriptomic, and proteomic analyses. Science **307:**82–86.
13. **Hiltpold, A., M. Frey, A. Hulsmeier, and P. Kohler.** 2000. Glycosylation and

palmitoylation are common modifications of *Giardia* variant surface proteins. Mol. Biochem. Parasitol. **109**:61–65.
14. **Hoek, J. B., and J. Rydstrom.** 1988. Physiological roles of nicotinamide nucleotide transhydrogenase. Biochem. J. **254**:1–10.
15. **Jackson, J. B.** 1991. The proton-translocating nicotinamide adenine dinucleotide transhydrogenase. J. Bioenerg. Biomembr. **23**:715–741.
16. **Jackson, J. B., S. J. Peake, and S. A. White.** 1999. Structure and mechanism of proton-translocating transhydrogenase. FEBS Lett. **464**:1–8.
17. **Kramer, R. A., L. A. Tomchak, S. J. McAndrew, K. Becker, D. Hug, L. Pasamontes, and M. Humbelin.** 1993. An *Eimeria tenella* gene encoding a protein with homology to the nucleotide transhydrogenases of *Escherichia coli* and bovine mitochondria. Mol. Biochem. Parasitol. **60**:327–331.
18. **Lee, Y.-N., L.-K. Chen, H.-C. Ma, H.-H. Yang, H.-P. Li, and S.-Y. Lo.** 2005. Thermal aggregation of SARS-CoV membrane protein. J. Virol. Methods **129**:152–161.
19. **Leon-Avila, G., and J. Tovar.** 2004. Mitosomes of *Entamoeba histolytica* are abundant mitochondrion-related remnant organelles that lack a detectable organellar genome. Microbiology **150**:1245–1250.
20. **MacMicking, J., Q. W. Xie, and C. Nathan.** 1997. Nitric oxide and macrophage function. Annu. Rev. Immunol. **15**:323–350.
21. **Mai, Z., S. Ghosh, M. Frisardi, B. Rosenthal, R. Rogers, and J. Samuelson.** 1999. Hsp60 is targeted to a cryptic mitochondrion-derived organelle ("crypton") in the microaerophilic protozoan parasite *Entamoeba histolytica*. Mol. Cell. Biol. **19**:2198–2205.
22. **Mann, B. J., B. E. Torian, T. S. Vedvick, and W. A. Petri, Jr.** 1991. Sequence of a cysteine-rich galactose-specific lectin of *Entamoeba histolytica*. Proc. Natl. Acad. Sci. U. S. A. **88**:3248–3252.
23. **Mann, B. J., C. Y. Chung, J. M. Dodson, L. S. Ashley, L. L. Braga, and T. L. Snodgrass.** 1993. Neutralizing monoclonal antibody epitopes of the *Entamoeba histolytica* galactose adhesin map to the cysteine-rich extracellular domain of the 170-kilodalton subunit. Infect. Immun. **61**:1772–1778.
23a. **Maralikova, B., V. Ali, K. Nakada-Tsukui, T. Nozaki, M. van der Giezen, K. Henze, and J. Tovar.** 2010. Bacterial-type oxygen detoxification and iron-sulfur cluster assembly in amoebal relict mitochondria. Cell. Microbiol. **12**: 331–342.
24. **McLane, M. W., G. Hatzidimitriou, J. Yuan, U. McCann, and G. Ricaurte.** 2007. Heating induces aggregation and decreases detection of serotonin transporter protein on Western blots. Synapse **61**:875–876.
25. **Meza, I.** 1992. *Entamoeba histolytica*: phylogenetic consideration. Arch. Med. Res. **23**:1–5.
26. **Mi-ichi, F., M. A. Yousuf, K. Nakada-Tsukui, and T. Nozaki.** 2009. Mitosomes in *Entamoeba histolytica* contain a sulphate activation pathway. Proc. Natl. Acad. Sci. U. S. A. **106**:21731–21736.
27. **Mitra, B. N., Y. Saito-Nakano, K. Nakada-Tsukui, D. Sato, and T. Nozaki.** 2007. Rab11B small GTPase regulates secretion of cysteine proteases in the enteric protozoan parasite *Entamoeba histolytica*. Cell. Microbiol. **9**:2112–2125.
28. **Nakada-Tsukui, K., Y. Saito-Nakano, V. Ali, and T. Nozaki.** 2005. A retromerlike complex is a novel Rab7 effector that is involved in the transport of the virulence factor cysteine protease in the enteric protozoan parasite *Entamoeba histolytica*. Mol. Biol. Cell **16**:5294–5303.
29. **Nakada-Tsukui, K., H. Okada, B. N. Mitra, and T. Nozaki.** 2009. Phosphatidylinositol-phosphates mediate cytoskeletal reorganization during phagocytosis via a unique modular protein consisting of RhoGEF/DH and FYVE domains in the parasitic protozoon *Entamoeba histolytica*. Cell. Microbiol. **11**:1471–1491.
30. **Nozaki, T., T. Asai, L. B. Sanchez, S. Kobayashi, and M. Nakazawa.** 1999. Characterization of the gene encoding serine acetyltransferase, a regulated enzyme of cysteine biosynthesis from the protist parasites *Entamoeba histolytica* and *Entamoeba dispar*. Regulation and possible function of the cysteine biosynthetic pathway in *Entamoeba*. J. Biol. Chem. **274**:32445–32452.
31. **Nozaki, T., T. Asai, S. Kobayashi, F. Ikegami, M. Noji, K. Saito, and T. Takeuchi.** 1998. Molecular cloning and characterization of the genes encoding two isoforms of cysteine synthase in the enteric protozoan parasite *Entamoeba histolytica*. Mol. Biochem. Parasitol. **97**:33–44.
32. **Okada, M., C. D. Huston, B. J. Mann, W. A. Petri, Jr., K. Kita, and T. Nozaki.** 2005. Proteomic analysis of phagocytosis in the enteric protozoan parasite *Entamoeba histolytica*. Eukaryot. Cell **4**:827–831.
33. **Okada, M., C. D. Huston, M. Oue, B. J. Mann, W. A. Petri, Jr., K. Kita, and T. Nozaki.** 2006. Kinetics and strain variation of phagosome proteins of *Entamoeba histolytica* by proteomic analysis. Mol. Biochem. Parasitol. **145**: 171–183.
34. **Riordan, C. E., J. G. Ault, S. G. Langreth, and J. S. Keithly.** 2003. *Cryptosporidium parvum* Cpn60 targets a relict organelle. Curr. Genet. **44**:138–147.
35. **Roger, A. J., S. G. Svard, J. Tovar, C. G. Clark, M. W. Smith, F. D. Gillin, and M. L. Sogin.** 1998. A mitochondrial-like chaperonin 60 gene in *Giardia lamblia*: evidence that diplomonads once harboured an endosymbiont related to the progenitor of mitochondria. Proc. Natl. Acad. Sci. U. S. A. **95**:229–234.
36. **Saito-Nakano, Y., T. Yasuda, K. Nakada-Tsukui, M. Leippe, and T. Nozaki.** 2004. Rab5-associated vacuoles play a unique role in phagocytosis of the enteric protozoan parasite *Entamoeba histolytica*. J. Biol. Chem. **279**:49497–49507.
37. **Salgado, M., J. C. Villagómez-Castro, R. Rocha-Rodríguez, M. Sabanero-López, M. A. Ramos, A. Alagón, E. López-Romero, and R. Sánchez-López.** 2005. *Entamoeba histolytica*: biochemical and molecular insights into the activities within microsomal fractions. Exp. Parasitol. **110**:363–373.
38. **Sambrook, J., and D. W. Russell.** 2001. Molecular cloning: a laboratory manual, 3rd ed. Cold Spring Harbor Laboratory Press, Cold Spring Harbor, NY.
39. **Sazanov, L. A., and J. B. Jackson.** 1994. Proton-translocating transhydrogenase and NAD- and NADP-linked isocitrate dehydrogenases operate in a substrate cycle which contributes to fine regulation of the tricarboxylic acid cycle activity in mitochondria. FEBS Lett. **344**:109–116.
40. **Stanley, S. L., Jr.** 2003. Amoebiasis. Lancet **361**:1025–1034.
41. **Tokoro, M., T. Asai, S. Kobayashi, T. Takeuchi, and T. Nozaki.** 2003. Identification and characterization of two isoenzymes of methionine γ-lyase from *Entamoeba histolytica*: a key enzyme of sulfur-amino acid degradation in an anaerobic parasitic protist that lacks forward and reverse trans-sulfuration pathways. J. Biol. Chem. **278**:42717–42727.
42. **Tovar, J., A. Fischer, and C. G. Clark.** 1999. The mitosome, a novel organelle related to mitochondria in the amitochondrial parasite *Entamoeba histolytica*. Mol. Microbiol. **32**:1013–1021.
43. **Tovar, J., G. Leon-Avila, L. B. Sanchez, R. Sutak, J. Tachezy, and M. van der Giezen.** 2003. Mitochondrial remnant organelles of *Giardia* function in iron-sulphur protein maturation. Nature **426**:172–176.
44. **Tovar, J., S. S. E. Cox, and M. van der Giezen.** 2007. A mitosome purification protocol based on Percoll density gradients and its use in validating the mitosomal nature of *Entamoeba histolytica* mitochondrial Hsp70. Methods Mol. Biol. **390**:167–177.
45. **van der Giezen, M.** 2009. Hydrogenosomes and mitosomes: conservation and evolution of functions. J. Eukaryot. Microbiol. **56**:221–231.
46. **van der Giezen, M., G. Leon-Avila, and J. Tovar.** 2005. Characterization of chaperonin 10 (Cpn10) from the intestinal human pathogen *Entamoeba histolytica*. Microbiology **151**:3107–3115.
47. **Vermeulen, A. N., J. J. Kok, P. Van Den Boogart, R. Dijkema, and J. A. J. Claessens.** 1993. *Eimeria* refractile body proteins contain two potentially functional characteristics: transhydrogenase and carbohydrate transport. FEMS Microbiol. Lett. **110**:223–229.
48. **Weston, C. J., J. D. Venning, and J. B. Jackson.** 2002. The membrane-peripheral subunits of transhydrogenase from *Entamoeba histolytica* are functional only when dimerized. J. Biol. Chem. **277**:26163–26170.
49. **Weston, C. J., S. A. White, and J. B. Jackson.** 2001. The unusual transhydrogenase of *Entamoeba histolytica*. FEBS Lett. **488**:51–54.
50. **Williams, B. A., R. P. Hirt, J. M. Lucocq, and T. M. Embley.** 2002. A mitochondrial remnant in the microsporidian *Trachipleistophora hominis*. Nature **418**:865–869.
51. **Yu, Y., and J. Samuelson.** 1994. Primary structure of an *Entamoeba histolytica* nicotinamide nucleotide transhydrogenase. Mol. Biochem. Parasitol. **68**:323–328.

International Journal for Parasitology 40 (2010) 833–843

Contents lists available at ScienceDirect

International Journal for Parasitology

journal homepage: www.elsevier.com/locate/ijpara

Members of the *Entamoeba histolytica* transmembrane kinase family play non-redundant roles in growth and phagocytosis

Sarah N. Buss [a,*], Shinjiro Hamano [b], Alda Vidrich [c], Clive Evans [d], Yan Zhang [d], Oswald R. Crasta [d], Bruno W. Sobral [d], Carol A. Gilchrist [e], William A. Petri Jr. [e]

[a] Department of Microbiology, University of Virginia, Charlottesville, VA 22908-1340, USA
[b] Department of Parasitology, Institute of Tropical Medicine (NEKKEN) and the Global COE Program, Nagasaki University, Nagasaki 852-8523, Japan
[c] Digestive Health Center of Excellence, Department of Medicine, University of Virginia, Charlottesville, VA 22908-1340, USA
[d] Virginia Bioinformatics Institute, Blacksburg, Virginia, 24061-0477, USA
[e] Division of Infectious Diseases and International Health, Departments of Internal Medicine, Microbiology and Pathology, University of Virginia, Charlottesville, VA 22908-1340, USA

ARTICLE INFO

Article history:
Received 13 November 2009
Received in revised form 15 December 2009
Accepted 17 December 2009

Keywords:
Entamoeba histolytica
Transmembrane kinase
Phagocytosis
Lectin
Laser-capture microdissection

ABSTRACT

Entamoeba histolytica contains a large and novel family of transmembrane kinases (TMKs). The expression patterns of the *E. histolytica* TMKs in individual trophozoites and the roles of the TMKs for sensing and responding to extracellular cues were incompletely characterised. Here we provide evidence that single cells express multiple TMKs and that TMK39 and TMK54 likely serve non-redundant cellular functions. Laser-capture microdissection was used in conjunction with microarray analysis to demonstrate that single trophozoites express more than one TMK gene. Anti-peptide antibodies were raised against unique regions in the extracellular domains of TMK39, TMK54 and PaTMK, and TMK expression was analysed at the protein level. Flow cytometric assays revealed that populations of trophozoites homogeneously expressed TMK39, TMK54 and PaTMK, while confocal microscopy identified different patterns of cell surface expression for TMK39 and TMK54. The functions of TMK39 and TMK54 were probed by the inducible expression of dominant-negative mutants. While TMK39 co-localised with ingested beads and expression of truncated TMK39 interfered with trophozoite phagocytosis of apoptotic lymphocytes, expression of a truncated TMK54 inhibited growth of amoebae and altered the surface expression of the heavy subunit of the *E. histolytica* Gal/GalNAc lectin. Overall, our data indicates that multiple members of the novel *E. histolytica* TMK family are utilised for non-redundant functions by the parasite.

1. Introduction

Cell surface receptors mediate the response to the environment across all forms of life. In metazoan organisms and plants, transmembrane kinases (TMKs) make up one of the major classes of cell surface receptors, with humans encoding about 80 TMKs (Manning et al., 2002) and *Arabidopsis thaliana* encoding over 400 (Champion et al., 2004; Shiu et al., 2004). The paradigm of receptor-mediated signalling governing cellular responses to environmental cues in plants and metazoa has not been fully extended to protozoa because protozoa have a general paucity of TMKs. However, examples of protozoan TMKs are beginning to be discovered and include nine predicted TMKs in *Dictyostelium discoideum* (Goldberg et al., 2006), 10 potential TMKs in *Trypanosoma brucei* (Parsons et al., 2005), 11 putative TMKs in *Plasmodium* (Ward et al., 2004), 88 predicted TMKs in *Monosiga brevicollis* (King and Carroll, 2001; Manning et al., 2008) and over 90 novel TMKs predicted in the protozoan parasite *Entamoeba histolytica* (Beck et al., 2005). The significance of these proteins remains unclear, as the majority have been characterised by sequence analysis only. A more complete understanding of protozoan TMKs will help define the mechanisms that these organisms use to respond to their environment and may shed light on the evolution of eukaryotic protein kinases.

The large family of novel TMKs identified in the *E. histolytica* genome has proposed roles in both amoebic response to the environment and immune evasion (Beck et al., 2005). *E. histolytica* is the causative agent of amoebiasis, a disease responsible for significant morbidity and mortality worldwide (WHO/PAHO/UNESCO, 1997). The parasite's biphasic life cycle consists of transmissible cysts and replicating trophozoites that colonise the lumen of the large intestine and occasionally invade the mucosa. Trophozoites must survey and adapt to the complex intestinal milieu and evade the immune system, but mechanisms that regulate the parasite's ability to persist for months within its human host remain incompletely understood.

* Corresponding author. Address: Division of Infectious Diseases and International Health, University of Virginia Health System, Carter Harrison Building Room 1711, 345 Crispell Drive, Charlottesville, VA 22908-1340, USA. Tel.: +1 434 924 8189; fax: +1 434 924 0075.
E-mail address: snb4k@virginia.edu (S.N. Buss).

0020-7519/$36.00 © 2010 Australian Society for Parasitology Inc. Published by Elsevier Ltd. All rights reserved.
doi:10.1016/j.ijpara.2009.12.007

In protozoan parasites such as *Giardia lamblia, Plasmodium falciparum* and *T. brucei*, antigenic variation, or the alteration of immunodominant surface antigens, is a common mechanism used to subvert host defences (Adam et al., 1988; Su et al., 1995; Stockdale et al., 2008). The process requires three elements: a large gene family encoding antigenically distinct surface proteins, expression of one variant antigen at a time by a single pathogen and a mechanism to switch the expressed gene (Borst and Genest, 2006). The *E. histolytica* TMKs have been implicated in the process of antigenic variation due to the nature of the gene family, the course of amoebic infection and observations made during transcriptional profiling studies (Beck et al., 2005). Additionally, some *E. histolytica* TMKs share sequence similarity with the variant-specific surface proteins (VSP) that are involved in the process of antigenic variation in *G. lamblia* (Beck et al., 2005).

It is possible that *Entamoeba* trophozoites undergo antigenic variation, as prolonged *E. histolytica* infections do occur (Haque et al., 2002) and antibody mediated protective immunity against *Entamoeba* is incomplete (Haque et al., 2001). However, trophozoites are known to use the process of capping, whereby antibody–antigen complexes are concentrated and released from the cell surface, as a means to avoid immune attack (Calderón et al., 1980). Additionally, amoebic trophozoites directly kill and ingest host cells, providing the organism with another mechanism for immune evasion (Ravdin et al., 1980). Nonetheless, it remains possible that the unusual TMK family may be involved with the process of antigenic variation. Real time PCR analysis of TMK expression by trophozoites during growth in culture revealed temporal changes in expression levels of some TMKs (Beck et al., 2005). As antigenic variation is known to occur without immune pressure (Roberts et al., 1992), the observed changes could be indicative of an antigenic switching event, where the averaging of population data masked expression of a single TMK by each cell.

Changes in TMK expression levels could also indicate that TMKs have specialised functions, as the TMKs have also been proposed to represent a major receptor system used by the cell to sense and respond to extracellular cues. The structural organisation of the *E. histolytica* TMKs suggests that they are type 1 integral membrane proteins, with signal-peptides, receptor-like extracellular domains and intracellular kinase domains, phylogenetically related to both S/T and Y kinases (Beck et al., 2005). When the TMKs were divided into nine sub-groups (A, B_{1-3}, C, D_{1-2}, E and F) based on signature motifs found within the substrate recognition regions of their kinase domains, similarity in the extracellular domains became apparent within sub-groups with respect to the size and the distribution of cysteine-rich motifs, suggesting that TMK sub-groups represent functionally distinct receptor families with sub-family-specific substrates and ligands (Beck et al., 2005). However, only two TMKs have been partially characterised to date: PaTMK (TMK-96, sub-family B_3) is expressed at the cell surface and functions in erythrophagocytosis (Boettner et al., 2008) and members of the B_1 family of TMKs play a role in proliferation and sensitivity to serum-derived growth factors (Mehra et al., 2006).

In this study, we sought to determine whether TMKs represent a gene family that undergoes antigenic variation or are an example of a protozoan TMK family that likely represents a major cell surface receptor system. We used laser-capture microdissection (LCM) and single cell microarray analysis and determined that a single amoeba expresses more than one TMK. To confirm expression of some TMKs at the protein level, anti-peptide antibodies were developed against TMK39 and TMK54. These TMKs were chosen because microarray data previously indicated that the genes were highly transcribed (amongst the TMKs) in both cultured and animal passaged trophozoites (Gilchrist et al., 2006), and TMK39 was identified at an early time point in a phagosomal proteome (Okada et al., 2006). We used the anti-peptide antibodies to stain cells for flow cytometric analysis and determined that the TMKs were homogenously expressed by trophozoites within a population. The antibodies were also used to localise TMK39 and TMK54 to discrete regions of the amoebic plasma membrane. We then utilised a functional genetic approach to demonstrate that TMK39 and TMK54 likely serve non-redundant cellular functions.

2. Materials and methods

2.1. Cultivation of E. histolytica and LCM

E. histolytica trophozoites, strain HM-1:IMSS, were grown axenically at 37 °C in complete TYI-S-33 medium containing 100 U/ml of penicillin and 100 μg/ml streptomycin (Invitrogen, Carlsbad, CA, USA) (Diamond, 1961). For all experiments, trophozoites were harvested during log-phase growth by a 10 min incubation on ice. For LCM analysis, harvested trophozoites were allowed to adhere to PEN foil-coated glass slides specifically designed for laser microdissection (Leica Microsystems, Bannockburn, IL, USA) for 15 min at 37 °C in TYI-S-33 media. Adherent trophozoites were sequentially fixed for 5 min in 70% and 100% ethanol followed by a few dips in xylene to completely dehydrate the samples and air-dried. Subsequently, single cells were captured from the PEN slides using the Leica AS LMD microdissection system (Leica Microsystems, Bannockburn, IL, USA). Captured cells were immediately processed as described below.

2.2. RNA isolation, amplification and microarray hybridization

RNA was purified from a single amoeba using the PicoPure™ RNA Isolation Kit (Molecular Devices, Sunnyvale, CA, USA) and the WT-Ovation™ Pico System (NuGEN, San Carlos, CA, USA) was used for cDNA synthesis and amplification. The quantity of cDNA obtained from one amplification cycle was insufficient for microarray analysis. Therefore one cycle amplified cDNA (1C) was subjected to a second cycle of amplification. Prior to microarray analysis, the linearity of the relationship between 1C and twice amplified cDNA (2C) was validated by quantitative reverse transcription PCR (qRT-PCR) (Section 2.4). 2C from a single cell was used for biotinylated cRNA synthesis. After biotinylation, 2 μg of cRNA was hybridized to the E_his-1a520285 Affymetrix custom array that has been described elsewhere (Gilchrist et al., 2006). The arrays were washed and stained with streptavidin–phycoerythrin (Molecular Probes, Carlsbad, CA, USA), following the standard Affymetrix protocol for eukaryotic targets (http://www.affymetrix.com/support/technical/manual/expression_manual.affx). The arrays were scanned with an Affymetrix Gene Chip scanner 3000 l and Affymetrix® GeneChip® Operating Software (GCOS) (http://www.affymetrix.com/products/software/specific/gcos.affx) was used to determine the detection call (present, marginal, or absent) for each probe set. The experiment was carried out in duplicate. Additionally, raw data from the arrays were normalised at the probe level by the gcRMA algorithm and then log2 transformed (Irizarry et al., 2003). The average log intensity values for all TMKs and for a few reference genes are listed in Supplementary Table S2. The complete microarray data was deposited in NCBI's Gene Expression Omnibus (Barrett et al., 2005) and is accessible through GEO Series accession number GSE19064 (http://www.ncbi.nlm.nih.gov/geo/query/acc.cgi?acc=GSE19064).

2.3. Genome analysis and datasets

The re-annotated *E. histolytica* genome, available at http://pathema.tigr.org, (GenBank accession number AAFB00000000) was used in this analysis.

2.4. qRT-PCR for validation of amplification and microarray

For validation of RNA amplification procedures, RNA from 10^6 *E. histolytica* trophozoites was prepared using the PicoPure™ RNA Isolation Kit and then subjected to either one or two cycles of amplification with the WT-Ovation™ Pico System. Two rounds of amplification yielded approximately 1.67 times more RNA than one round. 1C and 2C were adjusted to the same concentration and qRT-PCR was performed for 10 TMKs (TMK6, 56, 19, 60, 39, 63, 40, 65, 42 and 71) as previously described (Beck et al., 2005). See Supplementary Table S1 for primer sequences and annealing temperatures. The TMK threshold cycles (CTs) for 1C and 2C were then compared. As shown in Supplementary Fig. S1, 1C and 2C yielded similar CT values for all TMKs examined, indicating that the linearity of amplification was maintained throughout the second cycle.

For microarray validation, cDNA was prepared from a single cell as described above. The 2× amplified cDNA was diluted 1:100 with H_2O and qRT-PCR was carried out using iQSYBRGreen super mix (Bio-Rad, Hercules, CA, USA) and previously developed methods (Beck et al., 2005). Supplementary Table S1 lists primer sequences and annealing temperatures. Two "present" and two "absent" transcripts were selected for validation, and as a positive control cDNA was prepared from 10^6 trophozoites.

2.5. Antibodies

Peptides corresponding to amino acids (aa) 491–506 of TMK39 and 242–254 of TMK54 were synthesised, conjugated to Keyhole Limpet Haemocyanin and used to immunize New Zealand White rabbits. This work was contracted to Covance Research Products Inc., formal animal ethics approval was obtained and animal treatment was in accordance with all applicable laws and regulations. The resultant serum was affinity purified using immobilized peptide and dialysed against PBS. Resulting anti-TMK39 and anti-TMK54 antibodies were stored at −80 °C until use. Antibodies against TMK-96 (PaTMK) and the heavy subunit of the Gal/GalNAc lectin (Hgl) have been previously described (Petri et al., 1989; Boettner et al., 2008). Negative control, anti-Ft, an antibody which is directed against a *Francisella tularensis* protein, was a kind gift from Nicole Ark and Barbara Mann at the University of Virginia, USA. Polyclonal anti-actin (Santa Cruz Biotechnology, Santa Cruz, CA) and monoclonal anti-V5 (Sigma) antibodies were commercially available. For Western blotting, polyclonal antibodies were used at a concentration of 5 μg/ml, whereas monoclonal anti-V5 was used at 1 μg/ml. For confocal microscopy and flow cytometry antibody concentrations were doubled.

2.6. SDS–PAGE gels and Western blotting

Harvested trophozoites (HM-1:IMSS or induced HM-1:IMSS transfectants) were washed in PBS and lysed at a concentration of 10^4 amoebae/μL (50 mM Tris–HCl, pH 8.0, 150 mM NaCl, 1% Nonidet P-40, protease inhibitor cocktail (Sigma, St. Louis, MO, USA) and 0.02 mM E-64 (Sigma, St. Louis, MO, USA)). Cell lysate, immunoprecipitation or fractionated cellular sub-fractions (below) were resolved in 10% SDS–PAGE gels, transferred to polyvinylidene fluoride membrane using standard methods and membranes were blocked with 5% non-fat dry milk in Tris-buffered saline containing 0.1% (v/v) Tween-20 (TTBS) for 1 h at room temperature (RT). If noted, the membrane was cut into strips or primary antibodies (5 μg/ml) were pre-incubated with the indicated amount of unconjugated peptide for 1 h at RT prior to use. Primary antibodies diluted in TTBS were incubated with blocked membranes for 1 h at RT, membranes were washed with TTBS (5 × 5 min) and exposed to secondary antibody (anti-rabbit:AP or anti-mouse:AP) at a concentration recommended by the manufacturer (Sigma, St. Louis, MO, USA) for 1 h at RT. Finally, membranes were washed five times in TTBS and bands were visualised on film using the enhanced chemiluminescent (ECL) kit (Roche, Indianapolis, IN, USA).

2.7. Flow cytometry

Late-log phase *E. histolytica* trophozoites were harvested, washed twice with PBS and fixed with 3.7% paraformaldehyde (PFA) in PBS for 30 min at RT. If indicated, cells were permeabilized for 1 min with 0.2% Triton X-100 (Sigma, St. Louis, MO, USA) in PBS and non-specific binding was blocked by incubation with 20% goat serum and 5% BSA for 1 h at 37 °C. To assess TMK levels, permeabilized HM-1:IMSS trophozoites were stained for 1 h at 37 °C with anti-TMK39, anti-TMK54, anti-PaTMK (TMK-96), anti-Hgl (as a positive control) or anti-Ft (as a negative control).

To assess lectin levels, both non-permeabilized (cell surface Hgl) and permeabilized (total Hgl) transfected trophozoites were stained with anti-Hgl for 1 h at 37 °C. In both instances, Cy™ 3-conjugated Goat Anti-Rabbit IgG (Jackson Immuno Research, West Grove, PA, USA) was used as the secondary antibody at a 1:200 dilution in blocking buffer. As a control, cells were stained with secondary antibody only (no primary antibody). After 1 h incubation at 37 °C with the secondary antibody, samples were washed three times in PBS, re-suspended in 200 μl of PBS and analysed using a FACSCalibur (BD Biosciences) on channel FL2. In all instances, an intact amoeba gate was set prior to data collection (using side scatter (SSC) and forward scatter (FSC) and 10,000 gated events were collected for each sample. FlowJo software (http://www.treestar.com/flowjo/) was used for data analysis. All experiments were carried out three times or more and representative overlaid FL2 histograms are shown.

2.8. Fractionation

Cellular fractionation was carried out as previously described (Aley et al., 1980). Briefly, 10^8 trophozoites were harvested, washed twice with 19 mM potassium phosphate buffer, pH 7.2, and 0.27 M NaCl (PD). Cells were re-suspended to 2×10^7 amoebae/ml in PD + 10 mM $MgCl_2$ and mixed with an equal volume of 1 mg/ml concanavalin A in the same buffer. After 5 min at RT, cells were centrifuged at 50*g* for 1 min and the supernatant (containing excess conA) was discarded. The pellet was re-suspended in 12 ml of a hypotonic buffer containing 10 mM Tris–HCl, pH 7.5, 2 mM PMSF (Tris buffer) and 1 mM $MgCl_2$. After a 10 min swell, the cells were homogenised using 18–20 strokes of a glass Dounce homogenizer. A two-step gradient consisting of 0.5 M mannitol (8 ml) over 0.58 M sucrose (4 ml), both in Tris buffer, was prepared (gradient 1). The homogenate was layered on top and then centrifuged at 250*g* for 30 min. Large plasma membrane fragments formed a pellet at the bottom of gradient 1. The material remaining above gradient 1 was spun at 40,000*g* for 1 h to separate soluble cytoplasmic components (supernatant) from internal membranes (pellet). The plasma membrane pellet from the bottom of gradient 1 was re-suspended in 1 ml of Tris buffer + 1 M α-methyl mannoside and iced for 40 min with occasional mixing. The mixture was diluted into 3 volume of Tris buffer and homogenised with 80 strokes of a Dounce homogenizer. The homogenate was layered onto 20% sucrose in Tris buffer (gradient 2) and centrifuged at 250*g* for 30 min. Vesiculated plasma membranes that remained above gradient 2 were collected and concentrated by centrifugation at 40,000*g* for 1 h. The resulting pellet was re-suspended in Tris buffer and served as the plasma membrane fraction.

The three fractions used for analysis (soluble, internal membranes, and plasma membranes) were adjusted to equal volumes and analysed by Western blotting. As TMK39 and Hgl are similar in size (respectively, 127 kDa and 170 kDa), membrane panels

were first probed with anti-TMK antibodies and developed, then stripped with ReBlot Plus Strong Antibody Stripping solution (Millipore, Billerica, MA, USA) and re-probed with anti-Hgl antibodies.

2.9. Confocal microscopy

E. histolytica trophozoites (HM-1:IMSS) in TYI-S-33 medium were allowed to adhere to glass coverslips in a 24-well plate for 1 h at 37 °C at a concentration of 5.0×10^5 trophozoites/well. Adherent amoebae were washed with warm PBS and fixed with 3.7% PFA for 30 min at RT. Non-specific binding was blocked with 20% goat serum and 5% BSA (Sigma, St. Louis, MO, USA) in PBS (1 h at 37 °C). Cells were stained for 1 h at 37 °C with anti-TMK antibodies diluted in blocking buffer. If indicated, primary antibodies were pre-incubated with 300 nM unconjugated peptide for 1 h at RT. Cells were then washed three times with PBS and Cy3-conjugated goat anti-rabbit secondary antibodies (Jackson Laboratories, Bar Harbor, ME, USA) were added at a 1:200 dilution (in blocking buffer) for 1 h at 37 °C. After three washes, coverslips were mounted to slides with Fluoromount-G (Southern BioTech, Birmingham, AL, USA). A Zeiss LSM 510 laser-scanning microscope was used to visualise cells and final images were analysed using LSM Image Browser software (Carl Zeiss, Inc., Thornwood, NY, USA).

2.10. Inducible expression vectors

For expression of truncated proteins containing V5 and 6× His tags, the indicated regions of TMK39 and TMK54 were PCR amplified with the primers: 39F -CACC ATG TTT CTT TTA TTT ACA ATC CTC, 39R -AAT AAT AAT AAG AAT AAT CAC AAT CAG, 54F -CACC ATG TTG CTT CTT TTT TCA CTT ATT TCA, 54R -ACC AAG AAA TAT TAA AAT AGA TAA TAT AG. These fragments were cloned into the Gateway pENTR™/SD/D-TOPO® (Invitrogen) plasmid, sequence verified and Gateway® LR Clonase™ II Enzyme Mix (Invitrogen) was used, according to manufacturer's instructions, to transfer the truncated TMK fragments into the Gateway® pET-DEST42 vector in-frame with the C-terminal epitope tags. Truncated TMK fragments and tags were then PCR amplified from the pET-DEST42 vector with N-terminal *Kpn*I and C-terminal *Bam*HI restriction sites using the primers: K39F -CTA CTG GGT ACC ATG TTT CTT TTA TTT ACA ATC CTC, K54F -CTA CTG GGT ACC ATG TTG CTT CTT TTT TCA CTT ATT TCA, *Bam*HisR -ATA ATG GGA TCC TCA ATG GTG ATG GTG ATG ATG. Resulting PCR products were cloned into the *Kpn*I and *Bam*HI sites of the digested and gel purified pEhHYG-tetR-O-CAT vector (Hamann et al., 1997). Final constructs were sequence verified and the parental pEhHYG-tetR-O-CAT vector was used as a control.

2.11. Transfection of E. histolytica trophozoites

The GenElute™ HP Plasmid Maxiprep Kit (Sigma, St. Louis, MO, USA) was used to prepare plasmid DNA and DNA was quantified using the NanoDrop™ 2000 (Thermo Fisher, Wilmington, DE, USA). A known quantity of DNA was precipitated using standard methods and re-suspended to a concentration of 200 μg/ml in supplemented (5.7 mM cysteine, 25 mM HEPES and 0.6 mM ascorbic acid) and filter-sterilized Medium 199 (M199S) (Invitrogen, Carlsbad, CA, USA), that had been adjusted to pH 7.0. One hundred microlitre of the DNA (20 μg) was mixed with 15 μl of Attractene or SuperFect (Qiagen, Valencia, CA, USA) and incubated as per the manufacturer's instructions to allow formation of transfection complexes. Log-phase trophozoites were then harvested on ice, washed in M199S and re-suspended to a concentration of 5.0×10^5 amoebae/ml in M199S supplemented with 15% heat-inactivated bovine serum. Processed amoebae (0.9 ml) were added to transfection complexes and incubated for 3 h at 37 °C. After the incubation period, amoebae were added to 25 cm^2 tissue culture flasks containing complete TYI-S-33 medium supplemented with 100 U/ml of penicillin and 100 μg/ml streptomycin (Invitrogen, Carlsbad, CA, USA). After 18 h at 37 °C, transfected cells were selected using 15 μg/ml hygromycin (Invitrogen, Carlsbad, CA, USA). Debris from dead cells was removed and fresh media added beginning 4–5 days post-selection. Approximately 2 weeks after selection, transfectants obtained log-phase growth. Following 24 h of induction with 10 μg/ml of tetracycline, expression was verified by Western blotting using a monoclonal anti-V5 antibody (Sigma) as described.

2.12. Immunoprecipitation

Transfected cells were induced for 24 h and lysed on ice at a concentration of 10^7 amoebae/ml in 50 mM Tris–HCl, pH 8.0, 150 mM NaCl, 1% Nonidet P-40, protease inhibitor cocktail (Sigma, St. Louis, MO, USA) and 0.02 mM E-64 (Sigma). Cellular debris was removed by centrifugation at 9500*g* for 10 min at 4 °C. V5-agarose was washed in PBS five times and 20 μl of the washed agarose was added to 100 μl of cleared lysate. The mixture was incubated for 1.5 h at 4 °C on a shaker. Following the incubation period, the resin was washed three times in lysis buffer diluted 1:1 with PBS and twice in PBS. Twenty microlitre PBS and 5 μl 5× SDS–PAGE sample buffer were added to the agarose; the samples were heated to 95 °C for 10 min and analysed via Western blot.

2.13. Growth curves

Transfected (parental vector, t-39 or t-54) and non-transfected HM-1:IMSS trophozoites were harvested during log-phase growth and 10,000 cells were seeded into 15 ml of TYI-S-33 media that contained 10 μg/ml of tetracycline. Parasite numbers were recorded every 24 h for 4 days and expression of the protein was verified each day, in parallel. At least two independently transfected clones were tested, each sample was assayed in triplicate and results represent the mean of three or more experiments.

2.14. Amnis Imagestream data collection and analysis

Phagocytosis assays were carried out as described below, using 2×10^6 *E. histolytica* trophozoites and 2×10^7 carboxylate-modified 2.0 μm fluorescent yellow-green beads (Sigma, St. Louis, MO, USA). Following PFA fixation, amoebae were permeabilized with 0.2% Triton X-100 in PBS for 1 min if indicated and paraformaldehyde was neutralised with 50 mM NH_4Cl. Non-specific binding was then blocked by incubation (1 h at 37 °C) with 10% goat serum in PBS (blocking buffer). TMKs were detected by incubation for 1 h at 37 °C with anti-TMK antibodies diluted to 15 μg/ml in blocking buffer. Three PBS washes were performed and R-PE-conjugated goat anti-rabbit secondary antibodies (Jackson Laboratories, Bar Harbor, ME, USA) were added at a 1:200 dilution for 1 h at 37 °C. Following the incubation, samples were washed with PBS three times, re-suspended in 50 μl PBS and filtered through a 70 μm nylon cell strainer (BD Falcon, Bedford, MA, USA). Where indicated the procedure was carried out in the absence of amoebae (stained beads) or in the absence of anti-TMK antibodies (secondary only). At least 5000 images were collected using the Amnis Imagestream imaging cytometer (Amnis Corporation; Seattle, WA, USA) and ImageStream Data Exploration and Analysis Software (IDEAS) was used for data analysis. Prior to data analysis, spectral compensation was performed using "stained" beads and stained cells. Raw image files from the same experiment were all compensated with the same matrix and all compensated image files from the same experiment were opened with the same template. In each

template, gating was performed to generate a population of single, in-focus, bead-positive cell images (usually yielding 500–1000 images per sample) and masking was used to identify beads and the brightest 20% of antibody staining. Within the template, the Bright Detail Similarity (BDS) feature was used to calculate the extent of correlation between the two masks and thus quantify the extent of co-localisation between ingested beads and TMKs. BDS scores $\geqslant 3$ are considered co-localised.

2.15. Fluorescent labelling and killing of cells

Ficoll-Paque™ Plus (GE Healthcare, UK) isolated Jurkat cells or packed erythrocytes were suspended in 0.1% BSA in PBS at a concentration of 5×10^6/ml and incubated with 5 μM carboxyfluorescein succinimidyl ester (CFSE) for 10 min at 37 °C. FBS was used to quench unbound dye and the cells were washed three times with RPMI media. Jurkat cells were then killed using UV irradiation, whereas erythrocytes were calcium-treated by incubation at 37 °C for 48 h in HEPES buffer containing 2.5 mM $CaCl_2$. Both methods have been described elsewhere (Bratosin et al., 2001; Teixeira and Huston, 2008).

2.16. Phagocytosis assays

Phagocytosis was assayed by flow cytometry as previously described (Huston et al., 2003). Particles used for ingestion assays included fluorescent green 2.0 μm carboxylate-modified latex beads (Sigma, St. Louis, MO, USA), CFSE-labelled apoptotic Jurkat cells and Ca^{2+} treated red blood cells. Amoebae were induced with 10 μg/ml of tetracycline for 24 h. Particles were then mixed with amoebae at a 5:1 ratio, centrifuged for 5 min at 200*g* and incubated at 37 °C for 30 min. D-Galactose (110 mM) in ice-cold PBS was used to wash away non-ingested material and cells were fixed with 3.7% PFA. Samples were washed, re-suspended in PBS and analysed using a FACSCalibur (BD Biosciences) on channel FL1. SSC and FSC were used to distinguish amoebae from non-ingested particles and a live cell gate was established prior to data collection with 10,000 gated events collected for each sample. The mean fluorescence intensity (MFI) was calculated for each sample, background fluorescence was subtracted and data was plotted as a percentage of control MFI. Cell types were assayed in duplicate (at minimum) and the experiments were repeated at least three times. Data represents the mean of all experiments and error bars represent the SD.

2.17. Pinocytosis assay

Pinocytosis was assayed in a similar manner to phagocytosis, however 1 mg/ml FITC-dextran (Sigma) in PBS was incubated with amoebae instead of a particle. Incubation times and procedures were otherwise the same.

3. Results

3.1. Single cell TMK gene expression analysis

LCM was used in conjunction with microarray analysis to examine TMK gene expression at the single cell level. RNA isolated from a laser-captured *E. histolytica* trophozoite was subjected to two cycles of amplification and analysed via microarray (Supplementary Fig. S1). Affymetrix® GCOS was then used to generate detection calls for each TMK probe set. Multiple TMK transcripts were detected as present within a single cell (Table 1). The experiment was carried out in duplicate and TMK transcripts identified within both cells are underlined in Table 1. Average log intensity values for TMKs and reference genes are listed in Supplementary Table S2. Multiple TMK genes were expressed in both cells, and one cell expressed detectable levels of multiple members of TMK sub-groups A, B_1, D_1 and E. Microarray results were validated by qRT-PCR conducted on RNA isolated from an independently laser-captured trophozoite (data not shown). The presence of multiple TMK transcripts within a single cell indicated that these genes do not undergo antigenic variation at the level of transcription.

3.2. Protein expression analysis

To enable examination of TMK expression at the protein level, polyclonal antibodies directed against unique peptides within the extracellular domains of TMK39 (sub-family C) and TMK54 (sub-family E) were generated. Peptides were chosen for immunization by first manually identifying hydrophilic and cysteine-free stretches of sequence in each extracellular domain and then using the Basic Local Alignment Search Tool (BLAST) to check the sequences against the *E. histolytica* Genome Project Database and ensure specificity. Resultant antibodies were deemed specific as both recognised single bands of the predicted size in *E. histolytica* lysate and both bands disappeared when the antibodies were pre-incubated with increasing amounts of the corresponding unconjugated peptide (Fig. 1A). An anti-peptide antibody against PaTMK (TMK-96, sub-family B_3) has previously been developed and was also used in the following studies (Boettner et al., 2008).

Expression of PaTMK and sub-family B_1 TMKs has been examined at the protein level (Mehra et al., 2006; Boettner et al., 2008) however studies have been limited to Western blotting and microscopy. Consequently, it is unknown whether TMKs are heterogeneously expressed by trophozoites within a population. To examine expression of TMKs at the population level, we labelled permeabilized trophozoites with anti-TMK39, anti-TMK54 or anti-PaTMK, and analysed the samples by flow cytometry. In these experiments, trophozoites were harvested from the same flask, immediately fixed with 3.7% PFA and then stained. Flow cytometric

Table 1
Transmembrane kinase (TMK) transcripts detected in a single, *Entamoeba histolytica* trophozoite. Single cells expressed more than one TMK. RNA from a single amoeba isolated by laser-capture microdissection (LCM) was purified using the PicoPure™ RNA Isolation Kit and subjected to two cycles of amplification using the WT-Ovation™ Pico System. Resulting cDNA was hybridized to the E_his-1a520285 custom array (Affymetrix). The arrays were then stained using the standard Affymetrix protocol for eukaryotic targets. An Affymetrix Gene Chip scanner 3000 I was used to scan the arrays and report files were generated to determine the percentage of present calls. The experiment was carried out twice. TMK transcripts identified are listed, with those identified in both amoebae underlined. Validation of microarray results was carried out by quantitative reverse transcription PCR (qRT-PCR) (data not shown). cDNA samples used for microarray analysis and qRT-PCR validation were generated from different amoebae. For the validation, RNA was purified from a single cell and amplified (two rounds) as described. The mRNA abundance of two GCOS "present" (XM648585 and XM648643) and two GCOS "absent" (XM643895 and XM650501) transcripts was then measured by qRT-PCR. There was agreement in every instance.

TMK group	TMK#	GenBank XM#
A	TMK17	XM646584
	TMK23	XM647001
	TMK65	XM649022
B_1	TMK14	XM646638
	TMK87	XM644636
B_3	TMK35	XM645723
D_1	TMK03	XM646909
	TMK40	XM648928
D_2	TMK19	XM646939
E	TMK22	XM651330
	TMK54	XM648585
F	TMK06	XM644657
	TMK59	XM644333

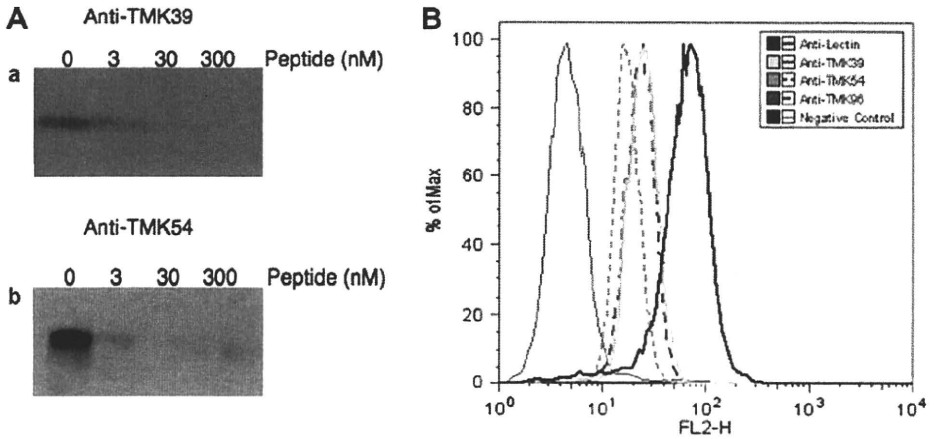

Fig. 1. Analysis of transmembrane kinase (TMK) protein expression in *Entamoeba histolytica* trophozoites. (A) Western blot with anti-peptide antibodies specific for TMK39 and TMK54. Lysate from 5.0×10^6 trophozoites was resolved in a large-well SDS–PAGE gel, transferred to polyvinylidene fluoride (PVDF) membrane and cut into strips. Each strip was incubated with 5 μg/mL of anti-TMK39 (a) or anti-TMK54 (b) that had been pre-incubated with the indicated amount of unconjugated peptide for 1 h at room temperature (RT). Anti-rabbit:AP (Sigma) was used for detection as recommended by the manufacturer. Antibodies recognised single bands of the expected size (127 kDa TMK39 and 100 kDa TMK54). (B) Populations of amoebae expressed more than one TMK. Permeabilized trophozoites were stained with antibodies against TMK39, TMK54, TMK-96 (PATMK), the Gal/GalNAc lectin or an irrelevant antibody (negative control) followed by an anti-rabbit:Cy3 conjugate. Flow cytometry was used to assess staining. Forward scatter (FSC) and side scatter (SSC) were used to gate on intact cells prior to data collection and 10,000 gated events were collected for each sample. The experiment was carried out three times and a representative histogram is shown.

analysis of the stained samples revealed homogenous expression of each TMK by more than 95% of cells within the population, compared with the anti-Ft negative control (Fig. 1B). The absence of distinct sub-populations strongly suggests that single amoebae express multiple TMKs at the protein level, further discounts the notion of antigenic variation, and points instead to the possibility of non-redundant function among TMK family members.

3.3. Localisation of TMK39 and TMK54

TMKs generally possess predicted signal-peptides of approximately 20 aa and single-pass transmembrane domains. Specific antibodies against PaTMK and cross-reactive antibodies against B_1 sub-family members have localised the corresponding proteins to punctate regions of the plasma membrane (Mehra et al., 2006; Boettner et al., 2008). As the cellular localisations of TMK39 and TMK54 are unknown, cellular fractionation and confocal microscopy were used to localise the two proteins in log-phase trophozoites. When an established method (Aley et al., 1980) was used to separate soluble, internal membrane and plasma membrane components, TMK39 and TMK54 were identified in both membrane fractions by Western blotting (Fig. 2A). As the proteins both contain canonical signal-peptides and membrane spanning regions, this was not surprising.

However, when TMK39 and TMK54 were localised using confocal microscopy, the pattern of plasma membrane staining in non-permeabilized cells was surprisingly different, with TMK39 in membrane microdomains (Fig. 2B). This difference was noticeable but less dramatic when the cells were permeabilized. In both instances, pre-incubation of the antibody (10 μg/ml) and corresponding peptide (300 nM) competitively inhibited the staining (Fig. 2B). The accumulation of TMK39 in discrete regions of the plasma membrane is reminiscent of membrane microdomains, such as aggregated lipid rafts and cavaolae that are thought to be centres of cell signalling in metazoan organisms (Parton and Hancock, 2004; Pike, 2006; Pani and Singh, 2009), as well as *E. histolytica* (Laughlin et al., 2004). In contrast, the even distribution of TMK54 throughout the plasma membrane mirrored the localisation of the *E. histolytica* Gal/GalNAc lectin (Petri et al., 1987). In permeabilized cells, both proteins were occasionally found associated with internal vesicles, however TMK54 was more consistently associated with some type of large intracellular compartment (Fig. 2B). While the biological significance of the proteins awaits further investigation, the distinct localisation patterns observed implied that TMK39 and TMK54 served non-redundant functions.

3.4. Functional analysis of TMK39 and TMK54

The kinase-containing intracellular regions of TMK39 and TMK54 were replaced with V5 and poly-histidine tags, and a tetracycline-inducible *E. histolytica* expression vector (Hamann et al., 1997) was used to over-express the truncated proteins, t-39 and t-54 respectively, in trophozoites (Fig. 3A). Parental vectors were transfected in parallel and served as a control for any unexpected effects of the induction of the tetO vector in the experiments. Each construct was used to generate at least two independently transfected clones. To confirm expression of the truncated proteins, cells were induced with 10 μg/ml of tetracycline for 24 h and cellular lysate was subjected to immunoprecipitation using anti-V5 agarose. The anti-peptide antibodies described above were used to probe Western blots of the immunoprecipitations, and both t-39 (Fig. 3B) and t-54 (Fig. 3C) cells expressed proteins of the expected size.

Importantly, wild type and truncated proteins appeared to interact, as endogenous TMK39 and TMK54 co-immunoprecipitated with the corresponding truncated protein (Fig. 3B and C). Receptor kinases are generally activated by ligand-induced dimerization followed by trans-autophosphorylation of kinase domains (Lemmon and Schlessinger, 1994; Heldin, 1995). Consequently, over-expression of dominant-negative receptors that lack cytoplasmic kinase domains has long been used to study the biological relevance of receptor kinases (Ueno et al., 1991). Such truncated receptors bind ligand, fail to propagate a downstream signal, and can inhibit wild type receptors through ligand-induced heterodimerization of the truncated and wild type proteins. These mutants therefore allowed us to address the biological functions of TMK39 and TMK54.

As shown in Fig. 4, cells induced to over-express t-54 had a severe growth defect during the first 24 h of induction but recovered to a near normal growth rate by 48 h (as indicated by the slope of

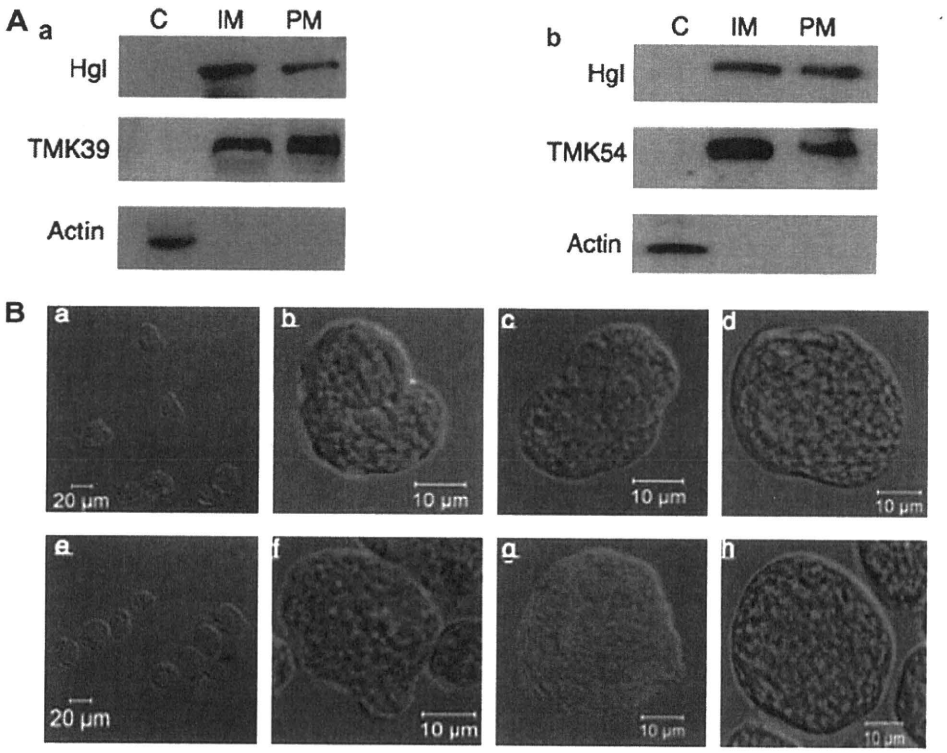

Fig. 2. Transmembrane kinases, TMK39 and TMK54 have discrete distributions at the cell surface. (A) *Entamoeba histolytica* trophozoites were lysed and fractionated. Trophozoite cytoplasmic (C), inner membrane (IM) and plasma membrane (PM) fractions were prepared for Western blot analysis. The panels were probed with anti-TMK39 (a) or anti-TMK54 (b), and in both instances, anti-Hgl and anti-actin antibodies were used as controls. Both TMK39 and TMK54 were expressed in membrane fractions. (B) Confocal images of non-permeabilized trophozoites are shown after staining with anti-peptide antibodies against TMK39 (a and b) and TMK54 (e and f). Permeabilized cells stained with anti-TMK39 (c) and anti-TMK54 (g) are also shown. As a control, antibodies were pre-incubated with the corresponding unconjugated peptides to competitively inhibit staining and staining with both anti-TMK39 (d) and anti-TMK54 (h) antibodies was abolished.

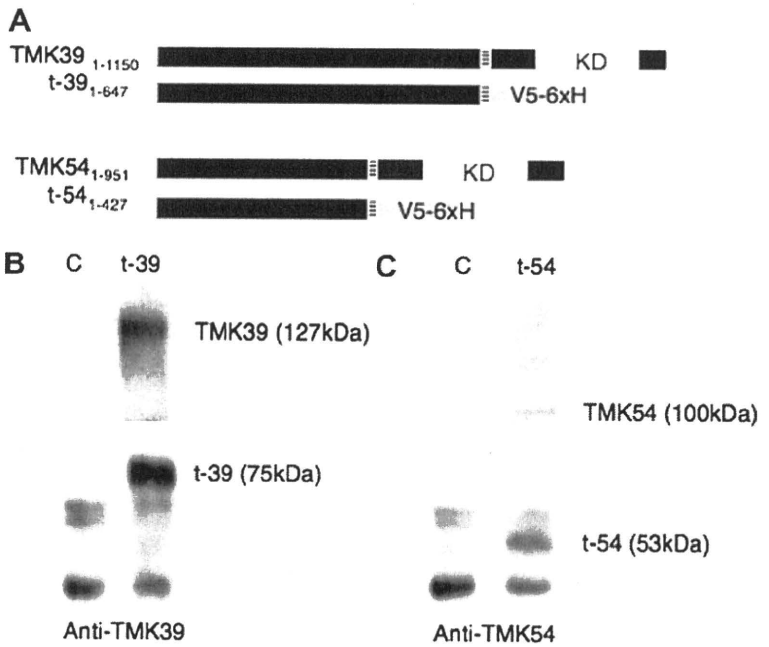

Fig. 3. Analysis of transmembrane kinase (TMK) function using a dominant-negative approach. (A) Depiction of the kinase domain (KD) deletions of TMK39 and TMK54 in t-39 and t-54, respectively. (B and C) Immunoprecipitation of t-39 and t-54. Amoebae were transfected with inducible expression vectors encoding t-39, t-54 or an empty vector control (C). Anti-V5 agarose was used to immunoprecipitate the truncated proteins from whole cell lysate. Western blots of immunoprecipitations are shown, probed with antibodies against TMK39 (B) or TMK54 (C). Heavy chain from the precipitating antibody is visible in every lane. As visualised, full-length wild type proteins co-immunoprecipitated with the truncated proteins in both instances. Separation between panels in B and C indicates different exposure times of blot to film.

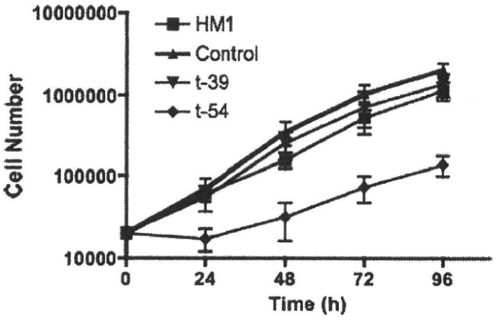

Fig. 4. Induction of t-39 and t-54 expression in *Entamoeba histolytica* trophozoites resulted in different phenotypes with respect to growth. Trophozoites were harvested during log-phase growth and 10,000 cells were seeded into media containing 10 μg/mL tetracycline. Cell numbers were assessed every 24 h for 4 days. For each construct at least two independently transfected clones were analysed. Each sample was assayed in duplicate and the graph represents the mean of three independent experiments +/− SD. For t-54 cells $P < 0.05$ at every time point after 0 h compared with any of the other cell types.

the line in Fig. 4). This was in contrast to t-39 cells, which had no defect. It is unclear how the t-54 cells were able to compensate for their growth defect.

To assess major cell surface changes in the mutant cell lines, flow cytometry was used to measure expression of the 170-kDa heavy subunit (Hgl) of the parasite's Gal/GalNAc lectin. After 24 h of induction, total levels of Hgl were comparable in t-39, t-54 and control cells (Fig. 5B), but the levels of surface expressed Hgl were significantly ($P < 0.05$) lower in t-54 cells (Fig. 5A).

Aside from this study, there is no published information available on the biological role of TMK54. However, TMK39 was identified at an early time point in an amoebic phagosomal proteome, and has therefore been implicated in the process of phagocytosis (Okada et al., 2006). To address the potential role of TMK39 in phagocytosis, we first assessed the extent of co-localisation between TMKs and ingested beads using multispectral imaging flow cytometry. Anti-peptide antibodies were used to stain trophozoites that had been allowed to ingest 2 μm carboxylate-modified fluorescent beads and samples were imaged using the Amnis Imagestream imaging cytometer. Beads were stained in an identical

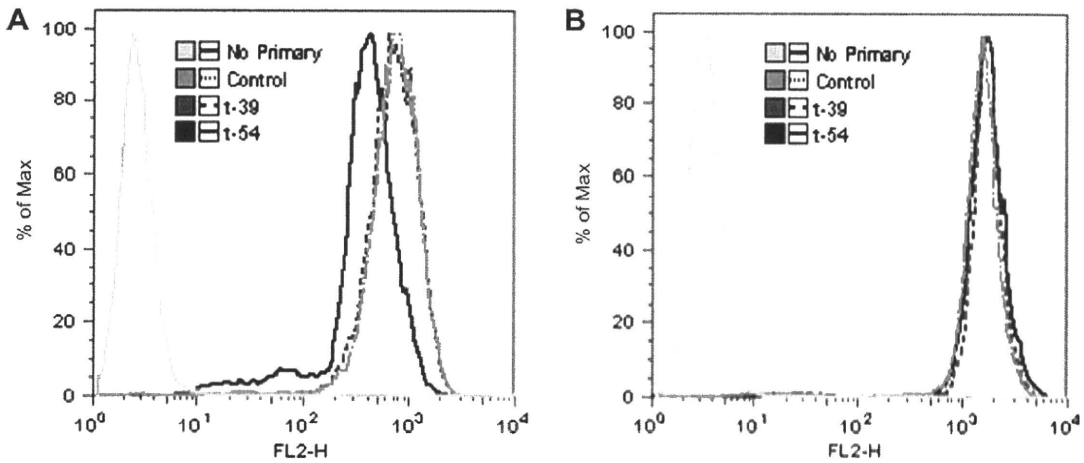

Fig. 5. Expression analysis of the heavy subunit of the Gal/GalNAc lectin (Hgl) in mutant *Entamoeba histolytica* trophozoites. t-39, t-54 and empty vector transfected cells were induced with 10 μg/mL tetracycline for 24 h, stained with anti-Hgl antibodies and assessed by flow cytometry. As a control, cells were stained with secondary antibody only (no primary). Prior to data collection forward scatter and side scatter were used to gate for intact cells and 10,000 gated events were collected for each sample. The experiment was repeated more than three times and representative histograms are shown for non-permeabilized (A) and permeabilized (B) cells. $P < 0.05$ for the mean fluorescence intensity (MFI) of non-permeabilized t-54 cells compared with the MFI of either control or t-39 cells.

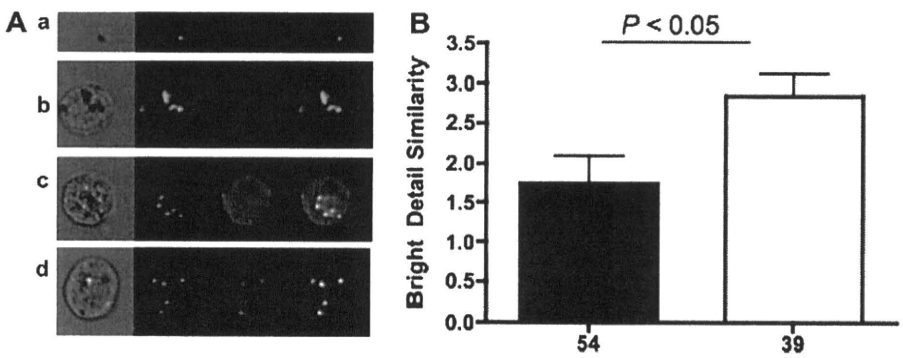

Fig. 6. Co-localisation of transmembrane kinase 39 (TMK39) with negatively charged beads during phagocytosis. Multispectral imaging flow cytometry was used to assess co-localisation at the population level. *Entamoeba histolytica* trophozoites were allowed to ingest carboxylate-modified beads, fixed and stained with anti-peptide antibodies. Beads were stained alongside bead-containing cells. Samples were imaged using the Amnis Imagestream imaging cytometer. (A) Representative images are shown for beads stained (as a control) with anti-TMK39 (a), permeabilized, bead-positive cells stained with secondary antibody alone (b), anti-TMK54 (c) or anti-TMK39 (d). (B) ImageStream Data Exploration and Analysis Software (IDEAS) was used to calculate the Bright Detail Similarity score (a measure of co-localisation between fluorescence in different channels with higher numbers indicating more co-localisation and a score ⩾ 3 indicating co-localisation) for permeabilized cells stained with anti-TMK39 and anti-TMK54, and results were plotted as mean Bright Detail Similarity (BDS) +/− SD for three independent experiments (*P*-value = 0.039).

manner to bead-containing cells to ensure that the anti-peptide antibodies and beads did not directly interact. While there was no evidence of non-specific binding of antibodies to beads, or of (as a control) co-localisation between TMK54 and ingested particles (Fig. 6A), TMK39 did appear to co-localise with ingested beads (Fig. 6A). Amnis IDEAS software was used to calculate the BDS score of single, in-focus, bead-positive cell images and the results are plotted in Fig. 6B as mean BDS +/− SD BDS scores are indicative of co-localisation between fluorescence in two channels: in this instance between ingested beads and TMKs. The mean BDS scores for permeabilized cells stained with TMK39 approached three (the accepted value for co-localised images) and TMK39 had higher BDS scores ($P < 0.05$), indicating a greater extent of co-localisation.

As TMK54 did not appear in any phagosomal proteome (Marion et al., 2005; Okada et al., 2006; Boettner et al., 2008) or co-localise with ingested beads, and as t-54 cells had striking defects in growth and surface expressed Hgl levels, the ability of t-54 cells to phagocytose was not assessed. However, flow cytometry was used to measure the ability of t-39 cells to ingest carboxylate-modified fluorescent beads, CFSE-labelled apoptotic Jurkat cells and Ca^{2+} treated erythrocytes. Uptake of FITC-labelled dextran was also measured as a marker of fluid phase pinocytosis. As shown in Fig. 7A and B, t-39 cells were significantly impaired in their ability to ingest carboxylate-modified beads and apoptotic Jurkat cells. The defect was specific, as t-39 cells were unimpaired in their ability to uptake FITC-dextran and Ca^{2+} treated erythrocytes.

4. Discussion

The most important conclusion from these studies is that single *E. histolytica* trophozoites express multiple members of a large TMK family and utilise the TMKs for non-redundant functions. While large families of TMKs have been considered hallmarks of multi-cellularity, the life cycle of *E. histolytica* provides clues as to why the protist would require an extensive network of cell surface signalling molecules. In the complex intestinal microenvironment, the organism must compete with bacteria for nutrients and space, sense stressors to regulate developmental changes between cyst and trophozoite, subvert host defences, ingest bacteria and control its invasive behaviour. Upon invasion, trophozoites continue to face a battery of challenges that require the ability to chemotax, adhere, kill and ingest human cells, and obtain sufficient nutrients. Survival of *E. histolytica* within its human host must require a profound ability to sense and respond to environmental challenges and utilisation of the extensive TMK network may therefore be critical.

Single cell microarray analysis demonstrated expression of multiple members of TMK sub-families A, B_1, D_1 and E. Expression of multiple sub-family members by a single cell raises the possibility that the TMK sub-families function in a complex manner similar to ErbB receptors in mammalian cells. ErbB family members form homo- and hetero-dimers, bind to different ligands and can be transactivated by other proteins (Linggi and Carpenter, 2006). It will be important to keep in mind the potential for such complexity while initiating preliminary studies on TMKs.

A limitation of this analysis was the minute quantity of RNA obtained from a single cell. Previous reports indicate that trophozoite populations in culture or isolated from mice cumulatively express 65–80% of *E. histolytica* genes (Gilchrist et al., 2006). However, only 15–20% of genes were detected as expressed within a single cell. While the averaging of population data in previous studies may have partially contributed to such a discrepancy, it is more likely that false-negative calls were generated in this study, as single cell microarray analysis is an inherently insensitive technique (Esumi et al., 2008), and members of the TMK gene family have been generally shown to be expressed at low to medium levels in other

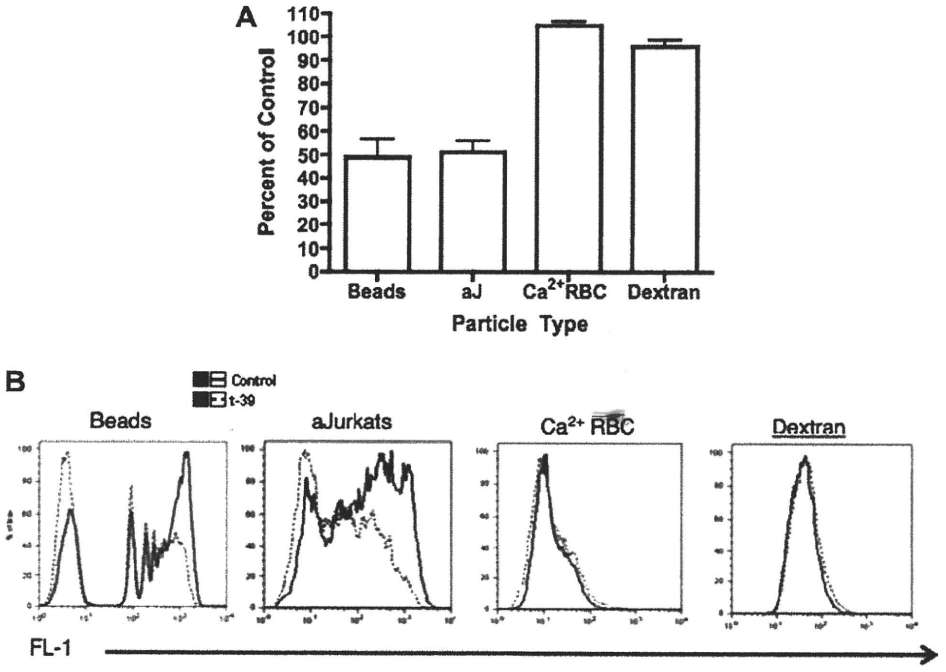

Fig. 7. Phagocytosis and pinocytosis in *Entamoeba histolytica* trophozoites induced to express t-39. (A) t-39 and empty vector transfected control cells were induced for 24 h with 10 μg/mL tetracycline and allowed to ingest carboxylate-modified beads, carboxyfluorescein succinimidyl ester (CFSE) labelled apoptotic Jurkat (aJ) cells, CFSE-labelled Ca^{2+} treated erythrocytes or FITC-labelled dextran. For each vector, at least two independently transfected clones were used in each experiment and the experiments were carried out more than three times. Samples were analysed by flow cytometry and the graph represents the mean fluorescent intensity (MFI) of t-39 cells plotted as a percentage of control cells. Error bars represent SD and $P < 0.005$ for beads and apoptotic Jurkats compared with either Ca^{2+} treated erythrocytes or dextran. (B) Representative histograms are shown.

studies (expression levels in prior studies are accessible through NCBI's Gene Expression Omnibus GEO Series accession numbers GSE8484, GSE13023, GSE6648, GSE6650). Moreover, TMK54 was detected as present by Affymetrix® GCOS (in both cells), but TMK39 and PaTMK were both GCOS absent in this study. In contrast, more than 95% of trophozoites within a population expressed each TMK at the protein level. Consequently, we believe that the single cell TMK transcriptome described in this study should be considered a minimal estimate.

Additional similarities between metazoan and *Entamoeba* TMKs are likely to exist. For example, the widely studied metazoan TMKs are activated by ligand-induced dimerization (Lemmon and Schlessinger, 1994; Heldin, 1995) and typically contain extracellular furin-like and/or epidermal growth factor – (EGF) like moieties. Furin-like domains are thought to be involved with the aggregation of metazoan receptor tyrosine kinases and EGF-like moieties contribute to protein–protein interactions. Although the pairing of TMK and EGF or furin-like domains is a rare occurrence in protozoa, many TMKs (including both TMK39 and PaTMK) possess cysteine-rich extracellular domains containing furin-like and/or EGF-like moieties. We observed hetero-dimerization between wild type and truncated receptors in this study, which may indicate that TMKs are subject to the same ligand-induced dimerization events as their metazoan counterparts.

Without identification of receptor ligand or kinase substrate, it is not possible to definitively ascribe functions to any of the TMKs that have been studied thus far. However, we have discovered a variety of clues that can help us begin to understand the function of these proteins. The striking difference in the surface localisation patterns of TMK39 and TMK54 was the first indication that these proteins served non-redundant functions. The uniform cell surface staining of TMK54 was similar to that of the heterotrimeric Gal/GalNAc lectin that mediates adhesion, cytotoxicity, phagocytosis and complement resistance (Petri et al., 2002). It is currently unknown how the Gal/GalNAc lectin orchestrates such a wide variety of events but sequence similarity between the short cytoplasmic tail of Hgl and the cytoplasmic tails of β2 and β7-integrins is considered to play a key role (Vines et al., 1998). Tyrosine phosphorylation of β-integrins stimulates their translocation to the cell surface (Naccache et al., 1994). Interestingly, t-54 cells expressed less Hgl on their surface compared with both t-39 and control cells, indicating that TMK54 may regulate Hgl surface expression. Additionally, t-54 cells had a striking growth defect during the first 24 h of t-54 protein induction, indicating that TMK54 may represent a major growth factor receptor. Cross-talk between growth factor receptors and integrins is also known to affect surface integrin levels (Somanath et al., 2009). Members of the B_1 family of TMKs have also been found to impact cellular proliferation but any impact on surface Hgl expression has not been described (Mehra et al., 2006). Future studies in our laboratory will address the biological role of TMK54 directly and examine the relationship between TMK54 and the Gal/GalNAc lectin.

In contrast to TMK54, TMK39 was localised to punctate regions of the plasma membrane, in a pattern reminiscent of membrane microdomains such as lipid rafts. As expected from its prior identification as a member of the phagosomal proteome (Okada et al., 2006), TMK39 was found to co-localise with ingested beads at the surface and to a greater extent within cells. Additionally, t-39 cells had a specific defect in their ability to ingest carboxylate-modified beads and apoptotic lymphocytes, but not Ca^{2+} treated erythrocytes. PaTMK has been previously shown to play a role in uptake of Ca^{2+} treated red blood cells (Boettner et al., 2008), providing additional evidence that TMKs serve non-redundant cellular functions. Considering previous studies that identified TMK39 as a component of the phagosomal proteome at early time points and the phenotype of t-39 cells, it is tempting to speculate that TMK39 may function as a scavenger receptor and mediate the internalisation of polyanionic macromolecules. Although phosphatidyl serine (PS) is a critical "eat-me" signal recognised by phagocytes (Grimsley and Ravichandran, 2003), it is unlikely that TMK39 recognises the molecule because recognition of exposed PS on the surface of aged or Ca^{2+} treated erythrocytes is known to impact uptake of red blood cells by *E. histolytica* (Boettner et al., 2005). Alternative "eat-me" signals, such as modified low density lipoprotein (LDL), are recognised by scavenger receptors that mediate the uptake of bacteria and apoptotic corpses in other systems (Grimsley and Ravichandran, 2003). TMK39 shares 30% identity with the *Drosophila* scavenger receptor eater across the first 200 aa of the proteins. Eater binds modified LDL and mediates uptake of bacteria, and the first 200 aa of eater are known to facilitate binding to polyanionic ligands (Kocks et al., 2005). Consequently, modified LDL is a candidate recognition signal for TMK39 and for *E. histolytica* phagocytosis of apoptotic lymphocytes.

In plants and metazoa, TMKs are known to regulate a myriad of cellular processes including cellular proliferation, survival, differentiation, migration, metabolism and host defence. This study suggests that TMKs are likely to mediate a similarly diverse and essential set of processes for this *E. histolytica*.

Acknowledgements

This work was supported by NIH grant 5RO1 AI026649 (to W.A. Petri) and Grant-in-Aid for Scientific Research (to S. Hamano).

Appendix A. Supplementary data

Supplementary data associated with this article can be found, in the online version, at doi:10.1016/j.ijpara.2009.12.007.

References

Adam, R.D., Aggarwal, A., Lal, A.A., de La Cruz, V.F., McCutchan, T., Nash, T.E., 1988. Antigenic variation of a cysteine-rich protein in *Giardia lamblia*. J. Exp. Med. 167, 109–118.

Aley, S.B., Scott, W.A., Cohn, Z.A., 1980. Plasma membrane of *Entamoeba histolytica*. J. Exp. Med. 152, 391–404.

Barrett, T., Suzek, T.O., Troup, D.B., Wilhite, S.E., Ngau, W., Ledoux, P., Rudnev, D., Lash, A.E., Fujibuchi, W., Edgar, R., 2005. NCBI GEO: mining millions of expression profiles – database and tools. Nucleic Acids Res. 33, D562–566.

Beck, D.L., Boettner, D.R., Dragulev, B., Ready, K., Nozaki, T., Petri, W.A., 2005. Identification and gene expression analysis of a large family of transmembrane kinases related to the Gal/GalNAc lectin in *Entamoeba histolytica*. Eukaryotic Cell 4, 722–732.

Boettner, D.R., Huston, C.D., Linford, A.S., Buss, S.N., Houpt, E., Sherman, N.E., Petri, W.A., 2008. *Entamoeba histolytica* phagocytosis of human erythrocytes involves PATMK, a member of the transmembrane kinase family. PLoS Pathog. 4, e8.

Boettner, D.R., Huston, C.D., Sullivan, J.A., Petri, W.A., 2005. *Entamoeba histolytica* and *Entamoeba dispar* utilize externalized phosphatidylserine for recognition and phagocytosis of erythrocytes. Infect. Immun. 73, 3422–3430.

Borst, P., Genest, P., 2006. Parasitology: switching like for like. Nature 439, 926–927.

Bratosin, D., Estaquier, J., Petit, F., Arnoult, D., Quatannens, B., Tissier, J.P., Slomianny, C., Sartiaux, C., Alonso, C., Huart, J.J., Montreuil, J., Ameisen, J.C., 2001. Programmed cell death in mature erythrocytes: a model for investigating death effector pathways operating in the absence of mitochondria. Cell Death Differ. 8, 1143–1156.

Calderón, J., de Lourdes Muñoz, M., Acosta, H.M., 1980. Surface redistribution and release of antibody-induced caps in entamoebae. J. Exp. Med. 151, 184–193.

Champion, A., Kreis, M., Mockaitis, K., Picaud, A., Henry, Y., 2004. *Arabidopsis* kinome: after the casting. Funct. Integr. Genomics 4, 163–187.

Diamond, L.S., 1961. Axenic cultivation of *Entamoeba histolytica*. Science, 134, 336-337.

Esumi, S., Wu, S., Yanagawa, Y., Obata, K., Sugimoto, Y., Tamamaki, N., 2008. Method for single-cell microarray analysis and application to gene-expression profiling of GABAergic neuron progenitors. Neurosci. Res. 60, 439–451.

Gilchrist, C.A., Houpt, E., Trapaidze, N., Fei, Z., Crasta, O., Asgharpour, A., Evans, C., Martino-Catt, S., Baba, D.J., Stroup, S., Hamano, S., Ehrenkaufer, G., Okada, M., Singh, U., Nozaki, T., Mann, B.J., Petri Jr., W.A., 2006. Impact of intestinal colonization and invasion on the *Entamoeba histolytica* transcriptome. Mol. Biochem. Parasitol. 147, 163–176.

Goldberg, J.M., Manning, G., Liu, A., Fey, P., Pilcher, K.E., Xu, Y., Smith, J.L., 2006. The *Dictyostelium* kinome – analysis of the protein kinases from a simple model organism. PLoS Genet. 2, e38.

Grimsley, C., Ravichandran, K.S., 2003. Cues for apoptotic cell engulfment: eat-me, don't eat-me and come-get-me signals. Trends Cell Biol. 13, 648–656.
Hamann, L., Buss, H., Tannich, E., 1997. Tetracycline-controlled gene expression in *Entamoeba histolytica*. Mol. Biochem. Parasitol. 84, 83–91.
Haque, R., Ali, I., Sack, R., Farr, B., Ramakrishnan, G., Petri, J., 2001. Amebiasis and mucosal IgA antibody against the *Entamoeba histolytica* adherence lectin in Bangladeshi children. J. Infect. Dis. 183, 1787–1793.
Haque, R., Duggal, P., Ali, I., Hossain, M., Mondal, D., Sack, R., Farr, B., Beaty, T., Petri, J., 2002. Innate and acquired resistance to amebiasis in Bangladeshi children. J. Infect. Dis. 186, 547–552.
Heldin, C., 1995. Dimerization of cell surface receptors in signal transduction. Cell 80, 213–223.
Huston, C.D., Boettner, D.R., Miller-Sims, V., Petri, W.A., 2003. Apoptotic killing and phagocytosis of host cells by the parasite *Entamoeba histolytica*. Infect. Immun. 71, 964–972.
Irizarry, R.A., Hobbs, B., Collin, F., Beazer-Barclay, Y.D., Antonellis, K.J., Scherf, U., Speed, T.P., 2003. Exploration, normalization, and summaries of high density oligonucleotide array probe level data. Biostatistics 4, 249–264.
King, N., Carroll, S.B., 2001. A receptor tyrosine kinase from choanoflagellates: molecular insights into early animal evolution. Proc. Natl. Acad. Sci. USA 98, 15032–15037.
Kocks, C., Cho, J.H., Nehme, N., Ulvila, J., Pearson, A.M., Meister, M., Strom, C., Conto, S.L., Hetru, C., Stuart, L.M., Stehle, T., Hoffmann, J.A., Reichhart, J., Ferrandon, D., Rämet, M., Ezekowitz, R.A.B., 2005. Eater, a transmembrane protein mediating phagocytosis of bacterial pathogens in *Drosophila*. Cell 123, 335–346.
Laughlin, R.C., McGugan, G.C., Powell, R.R., Welter, B.H., Temesvari, L.A., 2004. Involvement of raft-like plasma membrane domains of *Entamoeba histolytica* in pinocytosis and adhesion. Infect. Immun. 72, 5349–5357.
Lemmon, M.A., Schlessinger, J., 1994. Regulation of signal transduction and signal diversity by receptor oligomerization. Trends Biochem. Sci. 19, 459–463.
Linggi, B., Carpenter, G., 2006. ErbB receptors: new insights on mechanisms and biology. Trends Cell Biol. 16, 649–656.
Manning, G., Whyte, D.B., Martinez, R., Hunter, T., Sudarsanam, S., 2002. The protein kinase complement of the human genome. Science 298, 1912–1934.
Manning, G., Young, S.L., Miller, W.T., Zhai, Y., 2008. The protist, *Monosiga brevicollis*, has a tyrosine kinase signaling network more elaborate and diverse than found in any known metazoan. Proc. Natl. Acad. Sci. USA 105, 9674–9679.
Marion, S., Laurent, C., Guillén, N., 2005. Signalization and cytoskeleton activity through myosin IB during the early steps of phagocytosis in *Entamoeba histolytica*: a proteomic approach. Cell. Microbiol. 7, 1504–1518.
Mehra, A., Fredrick, J., Petri, W.A., Bhattacharya, S., Bhattacharya, A., 2006. Expression and function of a family of transmembrane kinases from the protozoan parasite *Entamoeba histolytica*. Infect. Immun. 74, 5341–5351.
Naccache, P., Jean, N., Liao, N., Bator, J., McColl, S., Kubes, P., 1994. Regulation of stimulated integrin surface expression in human neutrophils by tyrosine phosphorylation. Blood 84, 616–624.
Okada, M., Huston, C.D., Oue, M., Mann, B.J., Petri Jr., W.A., Kita, K., Nozaki, T., 2006. Kinetics and strain variation of phagosome proteins of *Entamoeba histolytica* by proteomic analysis. Mol. Biochem. Parasitol. 145, 171–183.
Pani, B., Singh, B.B., 2009. Lipid rafts/caveolae as microdomains of calcium signaling. Cell Calcium 45, 625–633.
Parsons, M., Worthey, E.A., Ward, P.N., Mottram, J.C., 2005. Comparative analysis of the kinomes of three pathogenic trypanosomatids: *Leishmania major*, *Trypanosoma brucei* and *Trypanosoma cruzi*. BMC Genomics 6, 127.
Parton, R.G., Hancock, J.F., 2004. Lipid rafts and plasma membrane microorganization: insights from Ras. Trends Cell Biol. 14, 141–147.
Petri, W.A., Chapman, M.D., Snodgrass, T., Mann, B.J., Broman, J., Ravdin, J.I., 1989. Subunit structure of the galactose and *N*-acetyl-D-galactosamine-inhibitable adherence lectin of *Entamoeba histolytica*. J. Biol. Chem. 264, 3007–3012.
Petri, W.A., Smith, R.D., Schlesinger, P.H., Murphy, C.F., Ravdin, J.I., 1987. Isolation of the galactose-binding lectin that mediates the in vitro adherence of *Entamoeba histolytica*. J. Clin. Invest. 80, 1238–1244.
Petri, W.A., Haque, R., Mann, B.J., 2002. The bittersweet interface of parasite and host: lectin–carbohydrate interactions during human invasion by the parasite *Entamoeba histolytica*. Annu. Rev. Microbiol. 56, 39–64.
Pike, L.J., 2006. Rafts defined: a report on the Keystone symposium on lipid rafts and cell function. J. Lipid Res. 47, 1597–1598.
Ravdin, J.I., Croft, B.Y., Guerrant, R.L., 1980. Cytopathogenic mechanisms of *Entamoeba histolytica*. J. Exp. Med. 152, 377–390.
Roberts, D.J., Craig, A.G., Berendt, A.R., Pinches, R., Nash, G., Marsh, K., Newbold, C.I., 1992. Rapid switching to multiple antigenic and adhesive phenotypes in malaria. Nature 357, 689–692.
Shiu, S., Karlowski, W.M., Pan, R., Tzeng, Y., Mayer, K.F.X., Li, W., 2004. Comparative analysis of the receptor-like kinase family in *Arabidopsis* and rice. Plant Cell 16, 1220–1234.
Somanath, P.R., Ciocea, A., Byzova, T.V., 2009. Integrin and growth factor receptor alliance in angiogenesis. Cell Biochem. Biophys. 53, 53–64.
Stockdale, C., Swiderski, M.R., Barry, J.D., McCulloch, R., 2008. Antigenic variation in *Trypanosoma brucei*: joining the DOTs. PLoS Biol. 6, e185.
Su, X., Heatwole, V.M., Wertheimer, S.P., Guinet, F., Herrfeldt, J.A., Peterson, D.S., Ravetch, J.A., Wellems, T.E., 1995. The large diverse gene family var encodes proteins involved in cytoadherence and antigenic variation of *Plasmodium falciparum* – infected erythrocytes. Cell 82, 89–100.
Teixeira, J.E., Huston, C.D., 2008. Participation of the serine-rich *Entamoeba histolytica* protein in amebic phagocytosis of apoptotic host cells. Infect. Immun. 76, 959–966.
Ueno, H., Colbert, H., Escobedo, J.A., Williams, L.T., 1991. Inhibition of PDGF β receptor signal transduction by coexpression of a truncated receptor. Sci., New Ser. 252, 844–848.
Vines, R.R., Ramakrishnan, G., Rogers, J.B., Lockhart, L.A., Mann, B.J., Petri Jr., W.A., 1998. Regulation of adherence and virulence by the *Entamoeba histolytica* lectin cytoplasmic domain, which contains a beta 2 integrin motif. Mol. Biol. Cell 9, 2069–2079.
Ward, P., Equinet, L., Packer, J., Doerig, C., 2004. Protein kinases of the human malaria parasite *Plasmodium falciparum*: the kinome of a divergent eukaryote. BMC Genomics 5, 79.
WHO/PAHO/UNESCO., 1997. A consultation with experts on amoebiasis. Mexico City, Mexico 28–29 January, 1997. Epidemiol. Bull. 18, 13–14.

IL-17 Is Necessary for Host Protection against Acute-Phase *Trypanosoma cruzi* Infection

Yoshiyuki Miyazaki,* Shinjiro Hamano,[†,‡] Seng Wang,* Yohei Shimanoe,* Yoichiro Iwakura,[§] and Hiroki Yoshida*

IL-17A is a key cytokine that induces inflammatory responses through the organized production of inflammatory cytokines, such as IL-6, TNF-α, and GM-CSF, and induces neutrophil migration. The roles of IL-17A in infection of intracellular protozoan parasites have not been elucidated, although augmented immune responses by IL-17A are important for the resolution of some bacterial and fungal infections. Therefore, we experimentally infected IL-17A–deficient (*IL-17A*$^{-/-}$) mice with *Trypanosoma cruzi*. *IL-17A*$^{-/-}$ mice had a lower survival rate and prolonged worse parasitemia compared with control C57BL/6 wild-type (WT) mice postinfection. In the infected *IL-17A*$^{-/-}$ mice, multiple organ failure was observed compared with WT mice, as reflected by the marked increase in serologic markers of tissue injury, such as aspartate aminotransferase, which resulted in increased mortality of *IL-17A*$^{-/-}$ mice. Expression of cytokines, such as IFN-γ, IL-6, and TNF-α, was lower in liver-infiltrating cells from the *IL-17A*$^{-/-}$ mice compared with WT mice. A similar defect was observed in the expression of neutrophil enzymes, such as myeloperoxidase and lipoxygenase, whereas cellular infiltration into the infected tissues was not affected by IL-17A deficiency. These results suggested that the efficient activation of immune-related cells critical for the killing of *T. cruzi* was impaired in the absence of IL-17A, resulting in the greater susceptibility of those mice to *T. cruzi* infection. From these results, we conclude that IL-17A is important for the resolution of *T. cruzi* infection. *The Journal of Immunology*, 2010, 185: 1150–1157.

Interleukin-17A is a proinflammatory cytokine, largely produced by activated T lymphocytes, and was originally called CTL-associated Ag-8 (1). The mouse IL-17 family consists of six members, including IL-17A (called IL-17), IL-17B, IL-17C, IL-17D, IL-17E (also called IL-25), and IL-17F, all of which share 16–45% homology with IL-17A (2). Among them, IL-17A and IL-17F are mainly produced by activated memory CD4$^+$ T cells, which are now classified as Th17 cells (3, 4). However, the production of IL-17A and IL-17F is not limited to Th17 cells; CD8$^+$ T cells, γδT cells, NK cells, and neutrophils have also been identified as sources of these cytokines (5–7). The receptor for IL-17A is expressed in various tissues, such as lung, kidney, liver, and spleen, and by various types of cells, including fibroblasts, epithelial cells, endothelial cells, monocytes/macrophages, lymphocytes, and marrow stromal cells. These cells produce diverse proinflammatory cytokines and chemokines in response to IL-17A stimulation (3). Yao et al. (8) reported IL-17A to be a potent inducer of IL-6 and IL-8 (CXCL8) by human fibroblasts. In subsequent experiments, it was shown that IL-17A could stimulate the expression of CSFs (G-CSF and GM-CSF), chemokines (CXCL1, CXCL10, CCL2, CCL7, and CCL20), and matrix metalloproteinase-3 and -13. These cytokines and chemokines augment local inflammations by inducing the recruitment of neutrophils and leukocytes. IL-17A also induces the production of IL-1β and TNF-α from macrophages (9), and these cytokines cooperate with each other to induce the production of IL-6 and chemokines (10, 11) and to augment inflammatory reactions (12).

Trypanosoma cruzi, an intracellular protozoan parasite, is the etiologic agent of American trypanosomiasis or Chagas' disease and affects ~16–18 million people in Central and South America (13). Innate and acquired cell-mediated immune responses are induced after experimentally induced acute *T. cruzi* infection, and combined mobilization of NK cells, CD4$^+$ T cells, CD8$^+$ T cells, γδT cells, and Ab-producing B cells are required for establishing host resistance (14, 15). Production of IL-12 by macrophages is triggered by the invasion of blood trypomastigotes of *T. cruzi* early postinfection, and IL-12 induces Th1 differentiation and subsequent IFN-γ production (16, 17). IFN-γ is a critical cytokine in host resistance to *T. cruzi* infection (18, 19); it is produced by NK cells at the early phase of infection and by CD4$^+$ and CD8$^+$ T cells later during the infection (20, 21). IFN-γ, synergistically with TNF-α, induces NO synthesis by macrophages, a critical mediator for killing of causal organisms during the acute phase of infection (22, 23). Furthermore, it is known that *T. cruzi* infection stimulates production of proinflammatory cytokines, such as IL-1α/β, IL-6, and TNF-α (24, 25). Infection-induced inflammatory reactions mediated by these cytokines against *T. cruzi* result in effective expulsion of the

*Division of Molecular and Cellular Immunoscience, Department of Biomolecular Sciences, Saga University, Saga; [†]Department of Parasitology, Graduate School of Medical Sciences, Kyushu University, Higashi-ku, Fukuoka; [‡]Department of Parasitology, Institute of Tropical Medicine and the Global Center Of Excellence Program, Nagasaki University, Nagasaki; and [§]Center for Experimental Medicine, Institute of Medical Science, University of Tokyo, Minato-ku, Tokyo, Japan

Received for publication January 7, 2009. Accepted for publication May 13, 2010.

This work was supported in part by grants from the Ministry of Education, Science, Technology, Sports and Culture of Japan (KAKENHI 19790363 and 21790474 to Y.M. and 19041059 and 21022038 to H.Y.); the Japan Research Foundation for Clinical Pharmacology; the Sumitomo Foundation, Grant for Basic Science Research Projects; the Naito Foundation; the Sankyo Foundation of Life Science; and the Takeda Science Foundation (all to H.Y.). This work was also supported by the president's expenditure (research project expenditure) of Saga University, Saga University Board of Trustees Award 2007, and grants-in-aid of The Japan Medical Association (all to H.Y.).

Address correspondence and reprint requests to Mr. Yoshiyuki Miyazaki, Division of Molecular and Immunoscience, Saga University, 5-1-1 Nabeshima, Saga 849-8501, Japan. E-mail address: miyazak4@cc.saga-u.ac.jp

The online version of this article contains supplemental material.

Abbreviations used in this paper: 5-LOX, 5-lipoxygenase; ALT, alanine aminotransferase; AST, aspartate aminotransferase; BUN, blood urea nitrogen; CK, creatine kinase; MLN, mesenteric lymph node; MNC, mononuclear cell; MPO, myeloperoxidase; ROS, reactive oxygen species; STA, soluble *Trypanosoma. cruzi* Ag; WT, wild-type.

www.jimmunol.org/cgi/doi/10.4049/jimmunol.0900047

parasites, although immunopathology from excessive inflammation also has a significant impact on the pathogenesis of experimental Chagas' disease (26, 27).

The roles of IL-17A in host defense against intracellular protozoan parasites remain to be fully elucidated, although IL-17A has a role in the host's protection against fungal and bacterial infection (28–31). Therefore, we investigated the role of IL-17A in *T. cruzi* infection. Infection by *T. cruzi* led to increased IL-17A production by $CD4^+$ T, $CD8^+$ T, NKT, and γδT lymphocytes. IL-17A–deficient (*IL-17A*$^{-/-}$) mice infected with *T. cruzi* exhibited more severe parasitemia and mortality accompanied by the attenuated production of antiparasitic cytokines, including IFN-γ, IL-6, and TNF-α, compared with wild-type (WT) mice. These results clearly indicated that IL-17A is necessary for the host's protection during acute-phase *T. cruzi* infection.

Materials and Methods

Animals

The generation of *IL-17A*$^{-/-}$ mice on the C57BL/6 background was described previously (32). Briefly, a targeting vector for deleting exons 1 and 2 of the *IL-17A* gene was electroporated into ES (E14.1) cells and selected in the presence of G418. Targeted clones, screened by Southern blot-hybridization analysis, were treated with adenovirus carrying the *cre* gene to delete the *neo* gene. Chimera mice were generated by the aggregation method, using C57BL/6 blastocysts as the recipients, and were mated with C57BL/6 female mice for germline transmission. Mutant mice were backcrossed onto the C57BL/6 background more than eight times (continual backcross) before use in experiments. Mice were housed in microisolator cages and were used between 8 and 12 wk of age. Age- and sex-matched WT C57BL/6 mice (Kyudo, Saga, Japan) were used as controls. All experiments were approved by the institutional animal research committee of Saga University and conformed to the animal care guidelines of the American Physiological Society.

Parasites

T. cruzi (Tulahuén strain) was maintained in vivo in *IFN-γR*$^{-/-}$ mice by every 2 wk passages. For the experiments, *IL-17A*$^{-/-}$ and WT mice were injected i.p. with the plasma containing trypomastigotes. Mice were infected with 2000 trypomastigotes. The number of parasites in the blood was counted for each animal using 4 μl venous blood. For measuring parasitism, DNA was purified from 50 mg tissue specimen with a Maxwell 16 Tissue DNA Purification Kit (Promega, Madison, WI). The content of infected parasites was measured with a PCR using *T. cruzi* 195-bp repeat DNA-specific primers TCZ-F: 5′-GCT CTT GCC CAC AAG GGT GC-3′ and TCZ-R: 5′-CCA AGC AGC GGA TAG TTC AGG-3′ (33). The PCR reaction was performed using SYBR Premix Ex Taq II (Perfect Real Time) (Takara, Shinga, Japan), according to the manufacturer's instructions (denaturation at 95°C for 30 s, followed by 40 cycles of the two-step amplification phase: 95°C for 5 s and then 60°C for 15-s hold). At the same time, we measured the level of murine *β2-microglobulin* gene as an internal control for DNA input using primers Beta2-F: 5′-TGG GAA GCC GAA CAT ACT G-3′ and Beta2-R: 5′-GCA GGC GTA TGT ATC AGT CTC A-3′.

Assay for serum chemistry

Blood was collected at indicated days postinfection, and serum was prepared by centrifugal fractionation. Serum alanine aminotransferase, aspartate aminotransferase, blood urea nitrogen, creatinine, and creatine kinase were determined using Test WAKO kit (Wako Pure Chemical Industries, Osaka, Japan), according to the manufacturer's directions.

Flow cytometric analysis

Prepared cells were stained with FITC-labeled anti-CD4 mAb, PE-labeled anti-CD62L mAb, and PE-Cy5–labeled anti-CD44 mAb (all from BD Biosciences, San Jose, CA) for the detection of effector $CD4^+$ T cells ($CD4^+/CD44^{high}/CD62L^{low}$) and PerCP-Cy5.5–labeled anti-CD69 mAb (BD Biosciences) for the detection of activated $CD4^+$ T cells ($CD4^+/CD69^{high}$). The following Abs against surface markers (BD Biosciences) were used to stain cells in the tissue: PE-labeled anti-CD4, FITC-labeled anti-CD8, PE-labeled anti-NK1.1, FITC-labeled anti-CD3, PE-labeled anti–Mac-1, FITC-labeled anti-B220, PE-labeled anti-Ly6G (1A8), FITC-labeled anti-neutrophils (7/4), and FITC-labeled anti–Gr-1 mAb. For the analysis of intracellular cytokines, the isolated cells (1×10^6) were cultured for 4 h with 10 ng/ml PMA (Sigma-Aldrich, St. Louis, MO) plus 500 ng/ml ionomycin (Sigma-Aldrich) in the presence of 2 μM monensin (Sigma-Aldrich) plus GolgiPlug (BD Biosciences). Cells were stained with FITC- or PE-labeled anti-CD4 mAb, FITC-labeled anti-CD8, NK1.1, γδ TCR, or Gr-1 mAb and PerCP or allophycocyanin-labeled anti-CD3 mAb (BD Biosciences), fixed, and permeabilized with the Cytofix/Cytoperm Plus kit (BD Biosciences), according to the manufacturer's directions. Cells were then stained with FITC-labeled anti–IFN-γ mAb or PE-labeled anti–IL-17 mAb (BD Biosciences). The expression of surface markers and cytokines was analyzed using FACSCalibur (BD Biosciences).

Histological analysis

Tissues were removed and fixed with 10% formaldehyde neutral buffer solution (Nacalai, Kyoto, Japan) at the indicated days after infection. Then, specimens were embedded in paraffin and stained with H&E, and structural changes and cellular infiltrations were evaluated with a light microscope.

In vitro assessment of IL-17A and Th17 function on macrophage and neutrophil activation

Spleen $CD4^+$ cells were isolated from WT or *IL-17A*$^{-/-}$ mice at 14 d after *T. cruzi* infection by MACS using anti-CD4 mAb. In contrast, peritoneal macrophages were collected from uninfected WT mice treated with 3% thioglycolate (Difco, Detroit, MI) for 3 d and seeded in 48-well culture plates at 5×10^5 cells/well. These macrophages were infected with 2.5×10^4 *T. cruzi* trypomastigotes and cocultured with the isolated WT or *IL-17A*$^{-/-}$ $CD4^+$ cells for 18 h. After the culture, cytokines and nitrite (NO) levels in culture supernatant were measured with the DuoSet ELISA Development System (R&D Systems, Minneapolis, MN) and the Griess Reagent Kit for Nitrite Determination (Molecular Probes, Eugene, OR), respectively. In another experiment, the thioglycolate-induced peritoneal exudate macrophages (5×10^5 cells/well) were treated with 25 ng/ml recombinant murine IL-17A for 18 h, and NO secretion was measured. NO production was also evaluated after stimulation with 100 ng/ml LPS, 25 ng/ml IFN-γ, or 1×10^6 soluble *T. cruzi* Ag (STA), with or without 25 ng/ml IL-17A. STA was prepared by repeated freeze and thaw of 1×10^8 trypomastigotes in 100 μl culture medium. For the preparation of neutrophils, peritoneal exudate cells were collected at 4–16 h after 3% thioglycolate injection. The cell suspension was put on 60% Percoll (GE Healthcare, Uppsala, Sweden) and centrifuged at 1000 × *g* for 30 min. The cell pellet, containing >80% neutrophils ($7\text{-}4^+Ly6G^+$ cells), was resuspended with culture medium and used in in vitro experiments as follows. The prepared neutrophils (5×10^5 cells) were treated with indicated stimuli, with or without recombinant mouse IL-17A (25 ng/ml) for 2 h. These cells were washed with PBS two times and then resuspended in PBS containing 10 μM 5-(and-6)-chloromethyl-2′, 7′-dichlorodihydrofluorescein diacetate (Invitrogen, Carlsbad, CA), a detection reagent for reactive oxygen species (ROS). After incubation for 30 min at 37° C in the dark, levels of ROS production were evaluated by flow cytometry. Induction of mRNA expression of myeloperoxidase (MPO) and 5-lipoxygenase (5-LOX) in the stimulated neutrophils for 16 h was analyzed by RT-PCR, as described below.

Isolation and culture of cells

Splenocytes, mesenteric lymph node (MLN) cells, and liver mononuclear cells (MNCs) were isolated from *IL-17A*$^{-/-}$ and WT mice at the indicated days after *T. cruzi* infection. Single-cell suspensions were prepared with a culture medium (RPMI 1640, Sigma-Aldrich) supplemented with 10% FBS (ThermoTrace, Melbourne, Australia) and penicillin/streptomycin (Invitrogen). Prepared cells (5×10^5 cells/well) were cultured in 96-well culture plates (Nunc, Roskilde, Denmark) for 3 d, and the culture supernatants were analyzed for cytokine production with ELISA, according to the manufacturer's directions (DuoSet ELISA Development System, R&D Systems).

Quantitative real-time PCR analysis

Total RNAs were extracted from cells using TRIzol reagent (Invitrogen) and reverse-transcribed with a ReverTra Plus kit (TOYOBO, Osaka, Japan). Expression levels of cytokines and neutrophilic enzymes were determined relative to that of β-actin with HotStar Taq DNA polymerase (Qiagen, Valencia, CA), supplemented with SYBR Green (Molecular Probes), using an ABI PRISM 7000 sequence-detection system, according to manufacturer's instructions. The sequence of PCR primers were as follows: IFN-γ, 5′-TCA AGT GGC ATA GAT GTG GAA GAA-3′ and 5′-TGG CTC TGC AGG ATT TTC ATG-3′; IL-4, 5′-ACA GGA GAA GGG ACG CCA T-3′ and 5′-GAA GCC CTA CAG ACG AGC TCA-3′; TNF-α, 5′-CAT CTT CTC AAA ATT CGA GTG ACA A-3′ and 5′-TGG GAG TAG ACA AGG

TAC AAC CC-3′; IL-6, 5′-GAG GAT ACC ACT CCC AAC AGA CC-3′ and 5′-AAG TGC ATC ATC GTT GTT CAT ACA-3′; MPO, 5′-ATC ACG GCC TCC CAG GAT ACA ATG-3′ and 5′-ACC GCC CAT CCA GAT GTC AAT G-3′; and 5-LOX, 5′-TGC CAT CCA GCT CAA CCA AAC-3′ and 5′-GCG ATA CCA AAC ACC TCA GAC ACC-3′.

Data analysis

Experiments were repeated at least two times. Values are expressed as mean ± SEM. Differences among groups were analyzed using unpaired Student *t* tests. A value of $p < 0.05$ was considered statistically significant.

Results

Induction of IL-17A expression by T. cruzi *infection*

First, we assessed IL-17A expression during *T. cruzi* infection. In uninfected mice, percentages of IL-17A–expressing cells were very low (<0.2%) in spleen and MLN. After *T. cruzi* infection, percentages of IL-17A–producing ($CD3^+CD4^+$ and $CD3^+CD4^-$) cells in spleen and MLN were increased; they reached a peak at 21 d after the infection and then decreased to basal levels (Fig. 1*A*). IFN-γ–producing cells also increased after *T. cruzi* infection as similar time-course in the case of IL-17A-producing cells (Fig. 1*A*). In contrast, although IL-17A–expressing cells existed in uninfected liver MNCs (~0.5%), the percentages were relatively constant during *T. cruzi* infection (Fig. 1*A*). Furthermore, $CD8^+$ T, NKT, and γδT cells in spleen, MLN, and liver also produced IL-17A against *T. cruzi* infection at 21 d after the infection (Fig. 1*B*). Therefore, it was demonstrated that *T. cruzi* infection induced production of IL-17A by various cell lineages.

High mortality accompanied by sustained severe parasitemia and aggravated multiple organ failure in IL-17A$^{-/-}$ mice

To clarify the role of IL-17A, we infected *IL-17A*$^{-/-}$ and WT mice with *T. cruzi*. As shown in Fig. 2*A*, the survival rate was markedly decreased in the *IL-17A*$^{-/-}$ mice compared with WT mice 21 d after the infection. In WT mice, expansion of the parasites showed a small peak at ~14 d postinfection but returned to sublethal levels in almost all mice (Fig. 2*B*). In contrast, *IL-17A*$^{-/-}$ mice showed prolonged, more severe parasitemia compared with WT mice up to 28 d after the infection (Fig. 2*B*). At 33 d postinfection, although the parasitemia in *IL-17A*$^{-/-}$ mice seemed similar to that in WT mice (†; Fig. 2*B*), this resulted from the fact that data were obtained only from a few survivors in the *IL-17A*$^{-/-}$ mice group. The survivors maintained the parasitemia at relatively milder levels than did others in the group during the acute phase of the infection, the parasitemia did not worsen again, and the mice

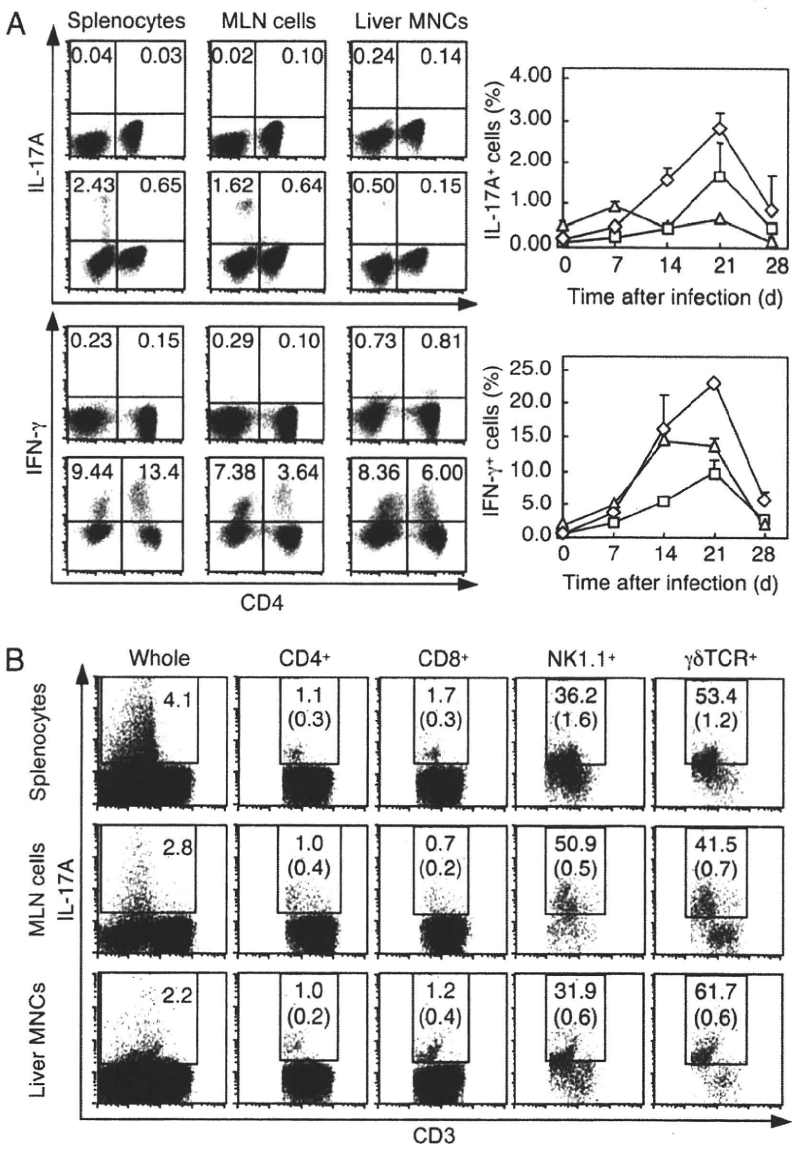

FIGURE 1. Induction of IL-17A from $CD4^+$ and other cell lineages during *T. cruzi* infection. *A*, *left panels*, Splenocytes, MLN cells, and liver MNCs prepared from WT mice on day 0 (*upper panels*) and day 21 (*lower panels*) of infection were stained for surface markers and intracellular IL-17A or IFN-γ and analyzed with FACS, as described in *Materials and Methods*. Numbers shown are the percentages of cells contained in gated $CD3^+$ cells. Experiments were repeated three times with similar results. *Right panels*, Splenocytes (◇), MLN cells (□), and liver MNCs (△) were prepared from WT mice at the indicated days postinfection, and the percentage of cells expressing IL-17A and IFN-γ was assessed. *B*, Splenocytes (*top row*), MLN cells (*middle row*), and liver MNCs (*bottom row*) collected from WT mice on day 21 of infection were stained for lineage surface markers and intracellular IL-17A. Numbers shown in each square are the percentages of the cells contained in each gated lineage; percentages of whole living cells are given in parentheses.